Title

Synaptic plasticity in the medial preoptic area of male mice encodes social experiences with female and regulates behavior toward young

Kazuki Ito[1], Keiichiro Sato[1], Yousuke Tsuneoka[2,3], Takashi Maejima[4], Hiroyuki Okuno[5], Yumi Hamasaki[1], Shunsaku Murakawa[1], Chihiro Yoshihara[2,6], Sayaka Shindo[2], Haruka Uki[1], Stefan Herlitze[7], Masahide Seki[8], Yutaka Suzuki[8], Takeshi Sakurai[9], Kumi O Kuroda[2,6], Masabumi Minami[1], Taiju Amano[1,2]*

[1] Department of Pharmacology, Graduate School of Pharmaceutical Sciences, Hokkaido University, 060-0812, Japan

[2] Laboratory for Affiliative Social Behavior, RIKEN Center for Brain Science, 351-0198, Japan

[3] Department of Anatomy, School of Medicine, Toho University, 143-8540, Japan

[4] Department of Integrative Neurophysiology, Graduate School of Medical Sciences, Kanazawa University, 920-8640, Japan

[5] Laboratory of Biochemistry and Molecular Biology, Graduate School of Medical and Dental Sciences, Kagoshima University, Kagoshima, 890-8520, Japan

[6] Dept. of Life Science and Technology, Tokyo Institute of Technology

[7] Department of General Zoology and Neurobiology, ND7/31, Ruhr-University Bochum, 44780, Germany

[8] Department of Computational Biology and Medical Sciences, Graduate School of Frontier Sciences, The University of Tokyo, 277-8562, Japan

[9] Faculty of Medicine/International Institute for Integrative Sleep Medicine (IIIS), University of Tsukuba, 305-8575, Japan

* **Correspondence to**: Taiju Amano, Department of Pharmacology, Graduate School of Pharmaceutical Sciences, Hokkaido University, Kita 12, Nishi 6, Kita-ku, Sapporo Hokkaido 060-0812, Japan Tel: +81-11-706-3246, Fax: +81-11-706-4987, E-mail: tamano@pharm.hokudai.ac.jp

Keywords:

paternal behavior, infanticide, aggression, social behavior, medial preoptic area, bed nucleus of the stria terminalis, electrophysiology

Summary

A dramatic shift from aggressive infanticidal to paternal social behaviors is an essential event for males after mating. While the central part of the medial preoptic area (cMPOA) has been shown to critically mediate the paternal behaviors in mice, how this brain region becomes activated by mating and subsequent interaction with pups has not been investigated. Here, we demonstrate that the reduction in inhibitory synaptic strength towards the cMPOA provided by posteriordorsal medial amygdala (MePD) neurons is a key event for the post-mating behavioral shift in males. Consistent with this, we found optogenetic disinhibition of Me^{Cartpt} to the cMPOA synapses reduces male aggression towards pups. We further provide evidence that the cMPOA of paternal mice mediated pup-induced neural plastic changes in the bed nucleus of the stria terminalis. These findings provide possible function of cMPOA neural circuits required for the reception to young in male mice.

Introduction

Reproductive behavior in male includes courting, mating and parental behavior. Polygynous male mammals, which form reproductive groups with one male and multiple females, often show aggressive behavior toward un-familiar infant conspecifics[1-5]. Infanticide of non-offspring young is commonly believed to improve reproductive success by achieving a shorter inter-birth interval for

51 females, a situation more favorable to breeding lower competition for resources, and the avoidance
52 of misdirected paternal investment[3,6]. After mating, however, the same male gradually stops
53 committing infanticide and becomes paternal, even toward non-biological offspring[5]. This behavioral
54 transition from infanticide to paternal care in C57BL/6 male mice is shown to require not only the
55 experience of ejaculation but also cohabitation with the pregnant female[7,8]. The exact neural
56 mechanisms governing this behavioral transition through social experiences with female and infant
57 remained unknown.

58 The medial preoptic area (MPOA) has been identified as one of the most important brain regions
59 regulating parental behavior[9]. Within the MPOA, the central part (cMPOA), located ventral to the
60 cluster of magnocellular oxytocin neurons (the anterior commissural nucleus), appears to play a pivotal
61 role in parental behavior because bilateral cMPOA lesions abolished this behavior and promoted
62 infanticide in both maternal and paternal mice[10,11]. Likewise, optogenetic activation of the MPOA in
63 virgin male mice delayed infanticidal behavior[11,12]. However, the neural circuit mechanisms that control
64 the MPOA neuronal activities was not clear. Previously, we reported that behavioral mode transition
65 from infanticide to parental was initiated by lesions of vomeronasal organ (VNO), which transmits
66 olfactory information to the accessory olfactory bulb[8]. Similar results were obtained in the experiment
67 using genetically mutated mice with impaired vomeronasal signaling[12]. Tracing studies using classical
68 retrograde tracer or rabies virus indicate that sensory information from accessary olfactory system is
69 mediated by the bed nucleus of the stria terminalis (BST) and the medial amygdala (Me) and is

transmitted to the MPOA[13-15]. It is reported that aggressive behavior toward pup is elicited by activation of GABAergic Me[16, 17].

The present study evaluates the efficacy of synaptic transmission from the Me to putative *Galanin*-positive cMPOA neurons from three groups: (i) males that experienced mating and pup exposure, (ii) males that experienced mating but had not pup exposure, and (iii) virgin males. We observed that inhibitory inputs from the Me to cMPOA were suppressed ahead of pup delivery, leading to cMPOA disinhibition. Optogenetic inhibition of Me−cMPOA synapses significantly reduced the proportion of mice showing aggressive behavior toward pups. Furthermore, we found paternal experiences increased synaptic inhibition in the rhomboid nucleus of the bed nucleus of the stria terminalis (BSTrh), one of a downstream structure of the MPOA[11]. Together, findings indicate that alterations in plasticity at Me–cMPOA synapses occur as a result of social experience with a female partner, which may function to prime a shift in behavioral response toward pups. This is followed by paternal experience with pups inducing changes in BSTrh.

Results

Sensitivity to GABAergic synaptic inputs from the Me to the cMPOA are suppressed by mating experience and cohabitation with a late gestational female

To map the projections from the Me to cMPOA, we took advantage of the high expression of the peptide, cocaine and amphetamine regulated transcript (Cart), in the subpopulation of posterior-

89 dorsal Me (MePD) neurons[18,19]. Within the Me, clusters of Cart-positive neurons were clearly
90 visualized in the MePD by immunostaining with an anti-Cart antibody (Figure S1A). We infused
91 biotin dextran amine (BDA), an anterograde neuron tracer, into the Cart-positive area of the Me
92 (Figure 1A and Figure B) and observed a projection to the cMPOA (Figure 1C and Figure S1B). The
93 cMPOA is located ventral to the anterior commissural nucleus, which contains magnocellular
94 oxytocin neurons and thus could be visualized using an antibody for the oxytocin-associated protein
95 neurophysin I (NPI)[10]. In contrast to the Cart-positive area of the Me, the Cart-negative area did
96 not send a dense projection to the cMPOA regardless of tiny BDA leak in Cart-positive area of the
97 Me (Figure S1C-F).

98 To address the cell-type in the cMPOA, the cMPOA neurons were manually collected using
99 a glass pipette and RNA-seq analysis was performed to evaluate mRNA expression levels. A six cell-
100 sample was combined and represented as data for one mouse. Here, we established three age-
101 matched experimental groups of male mice with different levels of paternal experience: 1) males
102 each co-housed with one female for mating, gestation, delivery, and remaining with the pups for the
103 first 3 postnatal days (paternal group), 2) males each co-housed with one female mating partner
104 until late gestation without exposure to pups (fathers in gestation experience; FGE group[20]), and 3)
105 virgin male mice. Table S1 lists the differentially expressed genes (DEGs) in cMPOA neurons among
106 virgin (V), FGE (F), and paternal (P) mice. Further, we evaluated the expression levels of 21
107 representative genes levels previously reported in activated MPOA neurons during social behavior[21]

108 to explore the recorded neuron's cell-type in this study and found no difference in their expression
109 levels among the groups (Figure 1D). Among all samples, expression level of *Galanin* (*Gal*) was the
110 highest. Previous studies have shown that the activation of Gal-Cre labeled MPOA neurons can
111 block infanticide in virgin male mice[12,14]. We visualized *Galanin* mRNA-positive neurons with
112 Alexa647 using *in situ* hybridization chain reaction (HCR). We observed a banded *Galanin*-
113 expressing region extending ventrally from the posterior part of the anterior commissure (AC) and
114 covering the cMPOA region (Figure 1E). Biocytin injected neurons during patch clamp recording
115 were visualized by reacting it with streptavidin conjugated to fluorescein isothiocyanate (FITC). We
116 observed that 85.0% (34 in 40 cells) of the recorded neurons were positive for *Galanin* mRNA co-
117 staining (Figure 1F and 1G). Meanwhile, Esr1, another marker gene in the MPOA region related to
118 parental behavior[21-23], was moderately detected among the groups (Figure 1D). Histological analysis
119 revealed that ERα-positive neurons (protein from the Esr1 translation) covered the cMPOA region,
120 which is locaged ventrally to NPI-positive neuronal clusters (Figure 1H). Compared with *Galanin*,
121 the ERα-positive neurons were broadly expressed in MPOA (Figure 1I). Further, 50% of patch clamp
122 recorded neurons (7 of 14 cells) were ERα positive (Figure 1J and 1K).

123 Next, to examine if social experience-dependent plastic changes in the cMPOA underlie the
124 shift from infanticidal to paternal behavior, we performed whole-cell patch clamp recordings of
125 cMPOA neurons from paternal, FGE, and virgin group mice to compare the synaptic responses.
126 There were no significant differences in passive membrane properties of cMPOA neurons among the

127 groups (Table S2 and S3). The projections including those from Cart-positive Me to the cMPOA were
128 electrically stimulated (Figure 1L), and the cell types of the recorded neurons were confirmed by post hoc *in situ*
129 hybridization staining. The average evoked inhibitory postsynaptic potential amplitude was
130 significantly smaller in the FGE group *Galanin*-positive cMPOA neurons compared with the virgin
131 group *Galanin*-positive cMPOA neurons (Figure 1M). A similar trend was observed in the
132 experiments in the blind targeted cMPOA neurons from the virgin and FGE groups (Figure S2A).
133 Considering that a high percentage of *Galanin*-positive neurons were targeted in the cMPOA
134 (Figure 1G), we considered that we were, in most cases, recording from *Galanin*-positive neurons.
135 Consequently, cell types are not discussed for each of the following experiments. Similar to FGE
136 mice, paternal mice showed a significant level of decreased eIPSP amplitude in the cMPOA
137 compared with the virgin mice (Figure 1N). We also addressed the effects of pregnant female
138 exposure alone (i.e., without the experience of copulation and delivery) on virgin males (virgin male
139 with late gestation; VMLG group, Figure S2B) or sexual experience without staying until late
140 gestation of female partner (male with mating experience; MME, Figure S2D). As a result, eIPSP
141 amplitude in the cMPOA in VMLG and MME mice were not changed (Figure S2C and S2E),
142 suggesting that either mating experience or cohabitation with a late gestational female was not
143 enough to reduce eIPSP amplitude in the cMPOA. To test the postsynaptic factors contribution to
144 plastic changes in paternal mice, a G-protein signaling blocker GDPβS was intracellularly infused.
145 The decreased eIPSP amplitude in the paternal group mice's cMPOA was reversed by GDPβS

146 intracellular infusion (Figure 1O). Collectively, these data suggested that mating and cohabitation
147 with a female, but not experience with pup, activates intracellular signals inducing disinhibition in
148 the cMPOA, which densely include *Galanin*-positive neurons.

149 Average evoked excitatory postsynaptic potentials (eEPSPs) amplitudes did not differ
150 between the groups (Figure 1P).

151

152 **Me^{Cartpt} neuron projections to cMPOA neurons are modified by female exposure alone**

153 To directly test if the eIPSP decrease observed in the cMPOA of FGE group mice is mediated by
154 input from Me neurons, we utilized Cartpt (which encodes Cart)-Cre mice. Cartpt-Cre × Ai9
155 reporter mice showed that 21.2% of NeuN-positive neurons in MePD were Cartpt (tdTomato)
156 positive (Figure 2A). We first infused an AAV vector encoding Cre-dependent eYFP into the Me of
157 Cartpt-Cre mice for pathway identification (Figure 2B). Indeed, we observed a clear Cre-dependent
158 eYFP expression in Me^{Cartpt} neurons and eYFP-labeled projections into the cMPOA (Figure 2C and
159 2D), consistent with the tracer study (Figure 1B and 1C). Next, we infused an AAV vector to express
160 blue light-sensitive channelrhodopsin, ChR2(H134R) in Me^{Cartpt} neurons and performed whole-cell
161 patch clamp recordings from cMPOA neurons in slices prepared from these mice. Application of blue
162 light to brain slices including the cMPOA depolarized the synaptic terminals derived from Me^{Cartpt}
163 neurons and induced both excitatory and inhibitory synaptic currents in cMPOA neurons (Figure 2E
164 and 2F), so we evaluated social experience-dependent synaptic changes at both excitatory and

165 inhibitory pathways. At the recording potential (−60 mV), glutamatergic and GABAergic ionotropic
166 receptor currents should flow in the opposite direction. Thus, glutamatergic and GABAergic
167 predominance can be distinguished by the net change in membrane current. Because of the
168 abundance of GABAergic neurons in the MePD[13], including retrogradely labeled cMPOA projecting
169 MePD neurons (Figure S3), we chose an experimental protocol that emphasized the EPSC
170 amplitude. The driving force for EPSC and IPSC, calculated by subtraction of the recording
171 potential (−60 mV) and reversal potential (−1 mV for EPSC, −87 mV for IPSC calculated by Nernst
172 equation), were about 59 mV and 27 mV, respectively. Under this experimental protocol, we counted
173 cMPOA neurons expressing predominantly blue light-induced EPSCs or IPSCs by the net
174 membrane current change. Whereas 83.3% of cMPOA neurons were IPSC-dominant in virgin male
175 mice, only 21.4% were IPSC-dominant in FGE males (Figure 2G). In accordance with the electrically
176 evoked responses (Figure 1O), intracellular perfusion of a G-protein signaling blocker GDPβS into
177 the cMPOA neurons reversed the ratio of IPSC- dominant neurons in FGE males to the level of
178 virgin males. As expected, control group mice expressing only eYFP did not show light-evoked
179 synaptic responses (Figure 2G). The data presented so far suggest that experiencing mating and
180 cohousing with a pregnant female impaired GABAergic synaptic transmission from Me^{Cartpt} into the
181 cMPOA.
182
183 **Optogenetic inhibition of Me-to-cMPOA inputs change the spontaneous synaptic activity**

184 To examine whether inhibition of Me^{Cartpt} terminals in the cMPOA modulate neural and/or
185 synaptic activity, we attempted to specifically silence these synapses. For this, we infused an AAV
186 vector encoding vertebrate long-wavelength opsin (vLWO)[24,25] bilaterally into the Me of virgin
187 Cartpt-Cre mice to suppress Me^{Cartpt} inputs (Figure 3A). To confirm the inhibitory effects of vLWO,
188 we performed whole-cell patch clamp recordings from Me^{Cartpt} neurons expressing vLWO-eGFP.
189 Application of green light hyperpolarized Me^{Cartpt} neurons (Figure 3B and 3C) but did not in the
190 control group (Figure 3D and 3E).

191 Next, we infused an AAV vector encoding ChR2 and vLWO into the Me of virgin Cartpt-Cre
192 mice to confirm the inhibitory effects of vLWO at the synaptic terminal (Figure 3F and 3G). After
193 more than 4 weeks, brain slices were prepared and recorded from cMPOA neurons. Green light
194 could affect ChR2 and therefore instead of using green light as above, red light was used to
195 stimulate the vLWO. The amplitude of blue light induced IPSC was significantly reduced by vLWO
196 activation (Figure 3H and 3I). Furthermore, the suppressed synaptic inputs from the Me^{Cartpt} to the
197 MPOA could result not only in reduced direct synaptic transmission but also in more frequent
198 inhibitory synaptic currents by disinhibition of surrounding interneurons. To address this
199 hypothesis, we observed spontaneous IPSCs (sIPSC) in each cMPOA neuron before and after the
200 suppression of inputs from the Me^{Cartpt} via vLWO activation (Figure 3J-L). Within 25 recorded
201 neurons, sIPSC frequency was increased more than 10% in 13 neurons and reduced more than 10%
202 in 1 neuron. The averaged frequency of the sIPSC in cMPOA was significantly increased (Figure 3L).

203 The application of tetorodotoxin (TTX) blocked the effects of vLWO activation (Figure 3M and 3N).

204 These data suggest that inhibition of the Me^{Cartpt} inputs to the MPOA could modify the activity of

205 each neuron in the cMPOA by acting on inter-neuronal network.

206

207 **In vivo optogenetic inhibition of Me-cMPOA inputs suppresses infanticidal behavior**

208 We previously demonstrated that Me neurons in infanticidal virgin males are highly activated and

209 express c-Fos protein following exposure to donor pups contained in wire mesh ball[8]. Consistent

210 with those results, in this study we observed that exposure of infanticidal virgin males to a pup in

211 wire mesh ball resulted in a significantly increased number of c-Fos- and eYFP-positive Me^{Cartpt}

212 neurons as compared with a wire mesh ball exposure alone (control) (Figure 4A-C).

213 Next, we aimed to address the causal relationship between synapse plastic changes in the

214 cMPOA and behavioral changes. To address the behavioral causality of the impaired Me-cMPOA

215 inputs, we infused an AAV vector encoding vLWO into the Me of virgin Cartpt-Cre mice and two

216 optic fibers were bilaterally implanted above the cMPOA for optogenetic stimulation. Green light

217 was delivered to the cMPOA during behaviors toward pups being observed (Figure 4D). The latency

218 to first sniffing did not differ significantly between the vLWO group and control group (Figure 4E).

219 However, the proportion of vLWO-expressing mice that did not show infanticidal behavior was

220 significantly larger than in the control group on 4 successive days (Figure 4F and 4G). After the 4-

221 day experiments with green light delivery, we examined the behavioral pattern toward pups

222 without green light delivery for some individuals. The proportion of vLWO group mice that showed
223 infanticidal behavior did not differ between day 4 (with light) and post-test (without light) (Figure
224 S4). Similar results were observed in the experiments, in which Me input to cMPOA was inhibited
225 in vGAT-IRES-Cre mice (Figure 5). Taken together, these data suggest that Me^{Cartpt} neurons
226 normally serve to suppress cMPOA neurons and promote infanticidal behavior.
227

228 **Paternal experience enhances inhibitory transmission in the BSTrh through a postsynaptic**
229 **mechanism**

230 We have demonstrated that the decreased inhibition of MPOA by Me input upon experiences with
231 female is a key event for suppressing the infanticide in the FGE. However, about half of FGE mice
232 still show the infanticidal behavior, whereas almost all paternal mice do not show infanticidal
233 behavior[8]. Next, we examined the synaptic change in paternal mice upon experiences with pup.

234 Downstream structure of the MPOA, the rhomboid nucleus of the bed nucleus of the stria
235 terminalis (BSTrh), has been shown to be activated by infanticidal behavior and negatively
236 regulated by cMPOA[11]. To address the impact of social experiences on the BSTrh synaptic property,
237 we measured the changes in the excitatory−inhibitory (E/I) ratio of the virgin, FGE and paternal
238 groups, in a manner similar to our previous studies[26]. The average amplitude of IPSPs evoked by
239 electrical stimulation of the stria terminalis (Figure 6A) was enhanced in the BSTrh of the paternal
240 group compared to FGE and virgin groups (Figure 6B). However, the average eEPSP amplitudes did

241 not differ significantly between these groups (Figure 6C). These data suggest that, in the paternal
242 mice, increased inhibition in the BSTrh critically takes place following the disinhibition in the Me–
243 cMPOA pathway as was seen in FGE mice.

244 We hypothesized that the cMPOA plays a critical role in the increase of inhibition in the
245 BSTrh. To evaluate this hypothesis, we specifically lesioned the MPOA. To this end, we bilaterally
246 injected NMDA into the cMPOA in virgin and paternal mice (Figure 6D and S5) and, 3 to 9 days
247 later, performed whole-cell recordings from BSTrh. In the BSTrh of ipsilaterally lesioned paternal
248 mice, the average eIPSP amplitude was significantly smaller than unlesioned paternal mice (Figure
249 6E). These data strongly suggest that the increased inhibitory input to the BSTrh is mediated by
250 the cMPOA in mice showing paternal behavior. It should be noted that cMPOA fiber inputs into
251 BSTrh were not likely stimulated to evoke synaptic responses in the current protocol because
252 cMPOA lesion unchanged eIPSP amplitude in virgin mice (Figure 6F).

253 We next addressed if this increased inhibition onto the BSTrh takes place through a pre- or
254 post-synaptic mechanisms. There were no significant differences in passive membrane properties
255 among the three groups (Table S4). We carried out patch-clamp analysis on BSTrh of paternal group
256 mice and found out that while an inclusion of the GDPβS in the pipette does reduce the amplitude of
257 eIPSPs to the level of virgin group (Figure 6G), eEPSP did not show obvious changes (Figure 6H).
258 These data suggest that the increased eIPSP amplitude in the BSTrh occurs mostly by postsynaptic
259 mechanisms. We also analyzed the paired-pulse ratios to compare the release probability from

260 presynaptic terminal and found out that the ratio of eEPSCs and eIPSCs did not differ between
261 paternal and virgin groups (Figure 6I). Altogether, we conclude that the cMPOA in the paternal
262 mice mediates plastic changes at GABA synapses in the BSTrh mainly by postsynaptic mechanisms,
263 and these sequential events are centrally involved in the fundamental switch in the paternal
264 behaviors of the father animals.

265

266 **Discussion**

267 The results showed that multi-step plastic changes in synapses correlate with the transition from
268 infanticidal to parental behavior in male mice. The inhibitory synapses from Me^{Cartpt} neurons in the
269 cMPOA were impaired by interactions with females. This plastic change in synapses is the potential
270 trigger for the behavioral transition from virgin to FGE. Our targeted cMPOA area are composed by
271 *Galanin*-positive neurons (Fig 1D-G), consistent with the previous reports that the activation of
272 *Galanin*-positive MPOA neuron cause inhibition of aggressive behavior toward pup[12,14]. In addition,
273 the shift from FGE to paternal was accompanied by an increased BSTrh inhibition. These plastic
274 changes caused the change of balance of excitatory–inhibitory synaptic transmission (E/I balance),
275 which correlated positively with the neuronal activity of the cMPOA and BSTrh, when virgin or
276 paternal males contacted with pups.

277 It was previously reported that the number of males showing infanticide decreased about
278 two weeks after ejaculation without cohabitation with the female partner[7,27]. This discrepancy may

279 be due to strain differences or by the different experimental/breeding environments. The behavior of
280 males toward pups appears to be controlled by factors triggered by ejaculation, which remain
281 effective for several subsequent weeks, thus preventing infanticide of the male's own offspring.
282 Followingly, additional mechanisms, such as activation of oxytocinergic neuron in paraventricular
283 nucleus of hypothalamus to initiate parental care[28], would complete a series of behavioral changes
284 of male, from aggression to parenting onset.

285 The Me has been implicated in various social behaviors, including social investigation,
286 mating, and aggression[29-33]. In males, the functional association between the Me and the MPOA is
287 critical for mating behavior[34,35]. The Me comprises several subdivisions with distinct projections and
288 cell types[36,37], including the MePD, which is a sexually dimorphic nucleus crucial for aggressive
289 behaviors[29,31,38,39]. We found the level of pup exposure-induced c-Fos expression in the VNO and
290 MePD was higher in infanticidal virgins than in paternal male mice[8]. On the other hand, the eIPSP
291 amplitude in cMPOA neurons of paternal mice elicited by the stimulation of axonal fibers derived
292 from Me was reversed by intracellular GDP-βS infusion (Figure 1O). These data suggest that both
293 decreased efficacy in synaptic transmission in cMPOA neurons, which we report, and hypoactivity of
294 MePD neurons likely contribute to behavioral selection in male mice. However, the notion that the
295 decrease of Me-to-cMPOA inputs in paternal mice causes a behavioral transition from infanticide to
296 parenting can be overly simplistic, since other brain areas should also provide inputs into the
297 cMPOA and can be modified by mating experiences. Further research is needed to elucidate this

298 phenomenon of behavioral transition in male mice.

299 Although we utilized Cartpt-Cre mice to map the Me−cMPOA pathway, Cart may function
300 as a neurotransmitter[40] and so influence Me to MPOA transmission. However, agonists and
301 antagonists specific for Cart transmission have not been identified, so we could not address the
302 influence of Cart released from the Me. In this study, we confirmed that manipulation of Me inputs to
303 the cMPOA in vGAT-IRES-Cre mice led to behavioral changes like those observed in Cartpt-Cre mice
304 (Figure 5). By considering data showing disinhibition in the cMPOA (Figure 1 and 2), we consider that
305 the plastic changes of GABAergic transmission at Me synapses strongly contribute to the shift from
306 infanticide to paternal behavior. On the other hand, we detected EPSCs by optical stimulation of Me
307 inputs into the cMPOA of Cartpt-Cre mice. Therefore, it is possible that subpopulation of Me neurons
308 might specifically control some cMPOA neurons and the associated behavioral pattern. The MPOA
309 contributes to several types of intrinsic behaviors, which in turn activate the MPOA according to
310 different patterns[11,23,32,33,41-44]. However, the mechanisms underlying the expression of one
311 appropriate behavior remains unknown. Suppressing the accessory olfactory signals mediating the
312 Me, presumably changes neural activity patterns in the cMPOA. This is supported by the results
313 that temporal disinhibition of the Me−cMPOA pathway modifies behavioral patterns and increases
314 cMPOA inter-neuronal network activity, as reflected by the increased frequency of postsynaptic
315 currents (Figure 3). In addition to the Me, other inputs into the cMPOA would drive several inter-
316 neuronal network activity patterns to achieve the multi-functional MPOA and behavioral choices.

317 Several studies report that activation of MPOA neurons in virgin males disturbs infanticide,
318 although parental behavior is not initiated[11,12]. Other studies report that activation of MPOA
319 neurons expressing Esr1 or afferents to ventral tegmental area (VTA) promotes parental behavior,
320 as measured by the latency to retrieve pups to the nest[22,23]. Here, the basal motivation for parenting
321 should be carefully distinguished from the behavioral choice toward the pups.

322 Uncovering the primary trigger of cMPOA plastic changes would promote the
323 understanding of how mammalians become parental. Neither mating nor cohabitation with a
324 pregnant female caused sufficient cMPOA disinhibition (Figure S2B and S2C). Because no
325 significant cMPOA disinhibition was observed in virgin males co-housed with a late-gestation
326 pregnant female (the VMLG group), the sensory inputs from pregnant females were unlikely to
327 induce synaptic changes in the cMPOA (Figure S2D and S2E). However, our cohabitation protocol
328 lasted only 3 days; it is possible that longer cohabitation is required for cMPOA disinhibition,
329 although longer cohabitation may be confused by the Bruce effect (i.e., spontaneous pregnancy
330 termination triggered by the scent of an unfamiliar male). Moreover, mating experience without
331 cohabitation with the female partner until late gestation did not change the GABAergic
332 transmission in the cMPOA. We are focusing on the previous reports that mating experiences
333 increase the dopamine turnover[45] and that plastic changes of the expression level of dopamine D_2
334 receptor in the MPOA were reported[46]. Because the function of dopamine receptors can change over
335 time[47,48], this may help explain the behavioral transition triggered by the social experience with

336 female partners. We observed that intracellular GDPβS infusion into cMPOA neurons reversed
337 eIPSP amplitude and the ratio of inhibitory- to excitatory-dominant neurons (Figure 1O, and 2G).
338 These data suggest that postsynaptic $GABA_A$ receptor activity on cMPOA neurons is downregulated
339 (i.e., neuronal disinhibition) by intracellular signals triggered in response to social experience with
340 females. Multiple signaling molecules are reported to be involved in the function of $GABA_A$
341 receptors[49]. Moreover, altered gene expression levels among virgin, FGE, and paternal mice were
342 recently reported[50]. Among them, the intracellular signaling molecules controlled by GPCR or small
343 G proteins are one of the possible targets to address the mechanisms of plastic changes in the
344 cMPOA.

345 Interestingly, unlike the synaptic changes in the Me^{Cartpt} - cMPOA pathways of FGE mice,
346 an inhibitory shift was observed in the BSTrh E/I balance, which was induced by the caring
347 experience (Figure 6). What is the biological significance of the increased BSTrh inhibition? Like
348 previous report[11], we observed that BSTrh inactivation by hM4Di significantly delayed infanticidal
349 behavior in virgin male mice without parental behavior initiation (Figure S6). This suggests that
350 BSTrh does not block parental behavior directly. Considering the time course for increased
351 inhibition between FGE and paternal mice, BSTrh plastic changes could contribute to pup
352 sensitization, which underlie the onset of pup caring. The cMPOA lesions reversed the increased
353 BSTrh inhibition in paternal mice to the level of virgin mice, suggesting that the inhibitory
354 transmission of BSTrh was controlled by cMPOA (Figure 6D and 6E). This is supported by the

355 following facts (1) cMPOA neurons project into the BSTrh and (2) unilateral lesion of the cMPOA
356 increases the number of c-Fos positive neurons in the ipsilateral BSTrh of mice exposed to pups[11].
357 Because of increased BSTrh inhibition in paternal mice is sensitive to intracellular GDPβS infusion
358 (Figure 6G), some metabotropic receptors of neurotransmitter or peptide may be influencing BSTrh
359 during and/or after pup sensitization. The cMPOA neurons activated during parental behavior
360 contain many kinds of neurotransmitters, including Galanin, neurotensin, and tachykinin2[10,51].
361 Moreover, the anterior commissural nucleus, adjacent to the cMPOA, contains the third largest
362 population of magnocellular oxytocin neurons. Therefore, cMPOA neurons or adjacent neurons may
363 directly and persistently control $GABA_A$ receptor activity in the BSTrh of paternal mice via
364 metabotropic receptors.

365 Converging data suggest that the cMPOA neurons contribute to both infanticide inhibition
366 and parental behavior by modifying the inter-neuronal network and projecting to the downstream
367 including BSTrh. There is no doubt that uncovering the relevant MPOA subgroup for each function
368 requires the analysis of neural circuits. Moreover, understanding the modulatory mechanism of
369 synaptic plasticity in the cMPOA and BSTrh may provide evidence for possible interventions in
370 parental stress and subsequent child maltreatment.

371

372 **Author contributions**

373 TA conceived the study with support from KOK. TA, TS and MM designed the experiments. TA, KI,

374 and KS conducted the behavioral experiments. TA and KI performed stereotaxic surgeries. TA, YT,
375 KI, KS, YH, SM and SS performed histological experiments. TA and HU performed whole-cell patch
376 clamp recordings. TM, TS and SH developed the AAV virus expressing vLWO. TA and HO prepared
377 sample for RNA sequence and YS, MS and KS analyzed data. TA wrote the manuscript with support
378 from KOK and YT. All authors contributed to editing the manuscript.
379

380 **Acknowledgements**

381 This work was supported by Japan Society for the Promotion of Science (JSPS) KAKENHI Grant
382 Number 25713044, 16K19747, 16H06279 (PAGS), 18K07584, 21K07494 (to TA), 26282220 (to KOK),
383 15K01832 (to TM), 19H03328, 20H05068 (to HO), Suzuken Memorial Foundation (to TA), Narishige
384 Neuroscience Research Foundation (to TA), Nishinomiya Basic Research Fund, Japan (to TA), and
385 the fellowship of Special Postdoctoral Researchers Program at RIKEN (to TA), Hokkaido University,
386 Global Facility Center (GFC), Pharma Science Open Unit (PSOU), funded by MEXT under "Support
387 Program for Implementation of New Equipment Sharing System," RIKEN Brain Science Institute
388 (2011-2015 to KOK), Deutsche Forschungsgemeinschaft He2471/18 Priority Program (SPP1926),
389 SFB874, SFB1280, DFG2471/21, DFG2471/23 project B10 (to SH). We appreciate Dr. Goichi Miyoshi
390 for critically reading this manuscript prior to submission, Dr. Shigeyoshi Fujisawa and Kazunari
391 Miyamichi for supporting genetically modified mice transportation, RIKEN Research Resource
392 Center for maintenance of animals, Kiyomi Imamura, Terumi Horiuchi, Dr. R. Jude Samulski and

the UNC Vector Core for helpful supports.

395 **STAR Methods**

396 Animals

397 The Animal Experiment Committee of the RIKEN Brain Science Institute and Institutional Animal
398 Care and Use Committee at Hokkaido University approved all animal experiments, which were
399 conducted in compliance with the National Institute of Health guidelines for the care and use of
400 laboratory animals.

401 Animal maintenance and male exposure to different levels of mating and paternal experience

402 Most C57BL/6J male mice were bred at the RIKEN Brain Science Institute and Graduate School of
403 Pharmaceutical Sciences, Hokkaido University unless specially described. For the BDA (Thermo
404 Fisher Scientific) tracer injection into Me (Figure 1A-C and S1), we utilized C57BL/6J male mice
405 from Japan SLC. Cartpt-Cre mice (Jackson Laboratory, stock number 009615), vGAT-IRES-Cre
406 mice (Jackson Laboratory, stock number 016962) and Ai9 (Jackson Laboratory, stock number
407 007909) were bred at the Graduate School of Pharmaceutical Sciences, Hokkaido University. We
408 backcrossed vGAT-IRES-Cre mice with C57BL/6J mice at least five generations after arrival from
409 Jackson Laboratory. Mice were housed in individually ventilated cages and provided ad libitum
410 access to water and food and maintained under a 12-h light/dark cycle in cages lined with TEK
411 Fresh Standard bedding (Envigo). Mice were weaned at postnatal day 28 (P28). All mutant
412 heterogenic mice were co-housed with wild-type mice until the experiments. To produce paternal
413 group mice, a virgin male mouse was housed with a female for mating. After delivery, the male

414 stayed with pups for 3 days. All paternal group males experienced one delivery and were used for
415 experiments within 20 days after the birth of pups. If pups did not survive for more than 3 days, the
416 male was not included in the paternal group for experiments. Other virgin male mice were mated
417 and co-housed with a female only until late gestation but not delivery, termed 'fathers in gestation
418 experience' (FGE) mice.
419
420 Stereotaxic surgery
421 BDA (1.25 μg/ dissolved in 12.5 nL 0.1 M phosphate buffer), N-methyl-D-aspartic acid (NMDA,
422 Sigma-Aldrich, 20 mg/ml in saline), and AAV5-EF1α-DIO-hChR2(H134R)-eYFP (6.6×10^{12} genome
423 copies/ml, provided by Vector Core at the University of North Carolina (UNC) at Chapel Hill, UNC
424 vector core), AAV5-EF1α-DIO-eYFP (5.6×10^{12} genome copies/ml, UNC vector core), AAV10-EF1α-
425 DIO-vLWO-eGFP-5HT1A (3.7×10^{13} or 1.8×10^{13} genome copies/ml, UNC vector core), AAV10-EF1α-
426 DIO-eYFP (1.2×10^{14} or 3.7×10^{13} genome copies/ml, UNC vector core), rAAV2-EF1a-DO_DIO-
427 tdTomato_EGFP-WPRE (more than 7.0×10^{12} vg/ml, Addgene), AAV2-hSyn-HA-IRES-eGFP ($3.3 \times$
428 10^{12} genome copies/ml, UNC vector core), and AAV2-hSyn-HA-hM4Di(Gi)-IRES-mCitrine (5.6×10^{12}
429 genome copies/ml, UNC vector core) (100–400 nL/hemisphere), were administered under anesthesia.
430 Briefly, 2–3-month-old male mice were anesthetized by intraperitoneal (i.p.) sodium pentobarbital
431 (30 mg/kg) or the mixture of medetomidine hydrochloride (0.3mg/kg), midazolam (4mg/kg),
432 butorphanol tartrate (5 mg/kg)[52], and local subcutaneous (s.c.) lidocaine hydrochloride. The skull

433 was exposed and holes drilled for stereotaxic injection. Glass capillaries of ~50 μm tip diameter were
434 filled with oil and backfilled with the test drug or AAV vector. Injection was targeted by referring to
435 the Mouse Brain Atlas of Flanklin & Paxinos (2007) coordinates for the Me (AP −1.5 mm, ML 2.1
436 mm, DV −5.4 mm and AP −1.2 mm, ML 1.9 mm, DV −5.6 mm), cMPOA (AP 0.1 mm, ML 0.55 mm,
437 DV −5.1 mm), and BSTrh (AP −0.1 mm, ML 1.2 mm, DV −4.2 mm). After injection, the skin was
438 closed with a nylon suture. Mice were kept in single housing 3−4 days for recovery. Mice injected
439 with AAV vectors were then maintained under group housing for more than 4 weeks to allow for
440 expression of vector genes. One week before behavioral testing, optic fibers were implanted into the
441 targeted area as described below.
442
443 Histological analysis
444 Mice were anesthetized by sodium pentobarbital (50 mg/kg, i.p.) and transcardially perfused with
445 4% paraformaldehyde (PFA) dissolved in phosphate buffered saline (PBS, pH 7.4). Brains were
446 removed from the skull and post-fixed overnight in PFA at 4 °C, followed by incubation in PBS/20%
447 sucrose for 1 day and PBS/30% sucrose for 1−2 days. Brains were then embedded in O.C.T.
448 Compound (Sakura Finetek) at −80 °C and sectioned at 40 μm using a Cryostat (Leica Biosystems)
449 unless otherwise indicated. Some brains were used to prepare sections for electrophysiological
450 analysis. In the case of BSTrh recording after MPOA lesion, serial slices including MPOA were
451 sectioned at 80 μm in cutting solution (see below) using a Leica VT1200 Semiautomatic Vibrating

452 Blade Microtome (Leica). These slices and the slices including BSTrh used for electrophysiological
453 analysis were fixed in 4% PFA and immunostained.

454 For fluorescent immunohistochemical staining, brain slices were incubated in PBS
455 containing 0.1% Triton X-100 (PBST) for more than 15 min and then in 0.4% Block Ace (Dainihon-
456 Seiyaku) for an hour. Slices were then incubated at 4 °C overnight in Block Ace solution containing
457 primary antibody. After several rinses in PBST, slices were incubated in PBST containing secondary
458 antibody at room temperature. Table S5 shows antibody list.

459 To stain the BDA anterograde tracer, sections were incubated with Alexa 568-conjugated
460 streptavidin (1:500, Thermo Fisher Scientific) for 2 hours. After washout of the secondary antibody
461 or streptavidin, slices were mounted on glass slides with VECTASHIELD Mounting Medium (Vector
462 Laboratories). For 3, 3-diaminobenzidine (DAB) staining, immunolabeled slices were incubated in
463 0.1 M glycine for 10 min, 0.5% H_2O_2 for 30 min, and VECTASTAIN ABC reagent (Vector
464 Laboratories) overnight at 4 °C. After rinsing several times with PBST, the slices were incubated
465 with Vector DAB Substrate (Vector Laboratories) including nickel chloride for about 5 min. The
466 stained slices were mounted on gelatin-coated glass slides and dried. After nissl staining, slides
467 were treated with Softmount (Wako). Labeling of *Galanin* positive neurons followed modified
468 protocol of *in situ* hybridization chain reaction (HCR) using short hairpin DNAs[53,54] using probes
469 listed in Table S6. Fixed brain section re-sliced at 75 μm after patch clamp recording with internal
470 solution containing 1% biocytin (Sigma) and 100 nU RNase inhibitor (Promega), or 30 μm brain

471 section fixed by 4% PFA were soaked in methanol for 10 minutes. After washing with PBST, the
472 sections were prehybridized for 10 min at 37°C in a hybridization buffer containing 10% dextran
473 sulfate, 1× standard saline citrate (SSC), 0.1% Tween 20, 50 μg/ml heparin, 1× Denhardt's solution.
474 The sections were moved to another hybridization solution containing a mixture of 20 nM split-
475 initiator probes, and incubated overnight at 37°C. For *in situ* HCR, 3 μM hairpin DNA solutions
476 were separately snap-cooled before use. The sections were incubated in amplification buffer (10%
477 dextran sulfate in 5× SSCT) with 60 nM hairpin DNA pairs for 2 hours at 25°C. Then, the samples
478 were washed with PBST three times at room temperature.

479 Immunofluorescence images were captured using an incident-light fluorescence microscope
480 (Leica DM6000B, Leica), confocal laser-scanning microscope (FV-10, Olympus), or fluorescence
481 microscope (BZ-X700, Keyence). To allow for comparison among trials, the contrast and brightness
482 of all photographs were adjusted linearly and uniformly using Adobe Photoshop CS5 (Adobe
483 Systems) unless specially described. For the lesion study, sections were immunostained with anti-
484 NeuN antibody to confirm cell death in the target area. The loss of NeuN-immunoreactive cells in
485 the NMDA-injected group was compared with the saline group to judge the lesioned area.

486

487 Electrophysiology

488 Electrophysiological recordings were performed as described previously[26]. The artificial cerebral
489 spinal fluid (ACSF) contained 126 mM NaCl, 2.5 mM KCl, 1.25 mM NaH_2PO_4, 1 mM $MgCl_2$, 2 mM

490 $CaCl_2$, 26 mM $NaHCO_3$, and 10 mM glucose (pH 7.3). For a cutting solution, NaCl in ACSF was
491 replaced with the same concentration of choline chloride. Mice were injected with pentobarbital (30
492 mg/kg, i.p.) followed by transcardiac perfusion of ice-cold cutting solution. The brains were removed,
493 and 230-μm brain slices including the target area prepared in ice-cold choline chloride-based cutting
494 solution using a Leica VT1200 Semiautomatic Vibrating Blade Microtome. Brain slices were stored
495 in warmed ACSF at 32 °C for 20–30 min and then kept at room temperature until recording.

496 For electrophysiological recordings, slices were superfused with 32 °C–34 °C ACSF at 2–4
497 mL/min in a chamber mounted on a microscope. Neurons were identified using a 40× or 60× lens
498 and an infrared camera (IR-1000, DEGE-MTI). Glass electrodes (World Precision Instruments) of 4–
499 9 MΩ resistance were used for whole-cell patch clamp recordings in response to electrical
500 stimulation using ~0.5 MΩ glass electrodes containing ACSF. Recording electrodes were filled with
501 a potassium-based internal solution (132 mM K-gluconate, 3 mM KCl, 10 mM HEPES, 0.5 mM
502 EGTA, 1 mM $MgCl_2$, 12 mM Na-phosphocreatine, 4 mM Mg-ATP, 0.5 mM Na-GTP, 0.2-0.3 %
503 biocytin, pH 7.25) and signals were recorded using an Axopatch 700B amplifier (Molecular Devices).
504 Only cells with access resistance <30 MΩ and exhibiting action potentials with >60 mV amplitude
505 evoked by positive current injection were included in the analysis. Whole-cell currents were filtered
506 at 3 kHz. The liquid junction potential (11 mV) was compensated. Stimulating electrodes were
507 placed at the dorsal BSTrh or cMPOA to stimulate stria terminalis. To activate the ChR2-expressing
508 axon terminals, we utilized a LED (465 nm, LEX2-LZ4-B, Brainvision Inc.). To activate the vLWO-

509 expressing neurons, green light generated by a 100 W mercury lamp (U-RFL-T) was applied
510 through a fluorescence band pass filter (520-550 nm) (Olympus). Red light was provided by Fiber-
511 Coupled LED (625 nm, Thorlabs). Evoked synaptic currents and potentials were measured at least
512 three times at the same stimulus intensity and averaged. Responses with action potentials were
513 omitted from the analysis. We recorded evoked excitatory postsynaptic potentials (eEPSPs) and
514 eEPSCs at a holding potential of −85 mV in the presence of 100 μM picrotoxin. eIPSPs were
515 recorded at −65 mV and eIPSCs at −60 mV in the presence of 20 μM CNQX and 20 μM MK-801. In
516 experiments using optogenetic suppression using vLWO, slices were also perfused with 25 μM 9-cis-
517 retinal, 0.1% dimethyl sulfoxide, 0.025% (±)- α-tocopherol and 0.2% bovine serum albumin.
518

519 Behavioral test

520 The tests of paternal behavior toward pups were performed as described previously[26]. Mice were
521 housed individually in cages containing new purified paper bedding (Alpha-Dri, Shepherd Specialty
522 Papers) and a cotton square (Nestlet, Ancare). After 1–2 days, three pups aged 1–6 days were placed
523 into the cage corner avoiding the nest. Tests were performed once each day for 30 min on 4
524 successive days during the daytime unless otherwise indicated. The endpoint of the aggressive
525 behavior toward pups to terminate the experiments was 2-s screams or visible wounds on the pup
526 skin. Wounded pups were immediately euthanized. The paternal behavioral score was evaluated
527 according to previous reports as follows: 4 = all pups were retrieved, 3 = 1 or 2 pups were retrieved,

528 2 = no pup was retrieved, 1 = at least one pup was attacked >3 min after placement in the test cage,

529 and 0 = at least one pup was attacked within 3 min after placement in the test cage.

530 For c-Fos mapping, the procedure was modified from a previous study[8]. Briefly, mice were

531 exposed to a pup protected inside wire-mesh ball (tea balls, 45 mm diameter; Minex Metal, Tsubame,

532 Japan) with about 10 holes (5 mm diameter) placed in a cage corner avoiding the nest for 30 min.

533 Ninety minutes later, the adult male was anesthetized with pentobarbital (50 mg/kg, i.p.) and

534 transcardially perfused with 4% PFA/PBS for brain isolation as described above. The c-Fos

535 immunoreactive cells were counted automatically by Image J software (National Institutes of

536 Health, Bethesda, MD, USA).

537

538 Optogenetic and chemogenetic manipulation of neural activity in vivo

539 Zirconia ferrules optical fibers (Thorlabs) of 200 μm diameter core (NA = 0.37) were cut and polished

540 for >70% coefficient of transmission. These constructs were bilaterally implanted into the mouse

541 brain area 1-mm above the target area and fixed with dental cement. After the mouse had recovered

542 from the surgery (one week later), the optic fibers were connected via Ceramic Split Mating with

543 1×2 Branching Fiber-optic Patch Cords-Glass (0.37 NA, Doric Lenses) to a diode laser (450 nm or

544 532 nm, Changchun New Industries Optoelectronics Tec.) through a FC/PC connector. Averaged

545 light power at the tips between the bilateral fiber tips was set to 30−40 mW (450 nm) or 10−12 mW

546 (532 nm). Light pulses were controlled by TTL Pulse Generators (Doric Lenses). After connecting

547 the fibers, experimental mice were allowed free actiTon for 15 min. During the last minute of the
548 behavioral test, mice received constant light on for 20 s without light pulses followed by a 10-s off
549 period. This photostimulation protocol was continued throughout the 30-min behavioral experiment.
550 After the behavioral experiments, animals were perfused with 4% PFA to prepare the brain slices.
551 Only animals with bilateral expression of fluorescence labeled fiber and the bilateral optic fibers
552 above targeted area between 0.3-1.0 mm from the targeted area were included for the data analysis.
553 For the chemogentic silencing, we infused CNO (2.0 mg / kg, i.p.) and observed the behavioral
554 pattern 30-35 min later. After the behavioral experiments, we immunostained the brain slices with
555 anti-GFP. Only animals with bilateral expression of fluorescent signal in the targeted area were
556 included for the data analysis.
557
558 RNA-seq analysis
559 Mouse brain slices were prepared using essentially the same procedures for electrophysiological
560 experiments. Six cMPOA neurons were manually collected by using 1 ~ 2 MΩ glass electrodes
561 containing ACSF and suspended in cell lysis buffer (0.5% Triton-X100, 0.5 U/μL RNase inhibitor, 5
562 ng/μL yeast rRNA). The cell samples were immediately frozen and stored at −80°C until starting
563 reverse transcription. Reverse transcription and cDNA library preparation were performed using
564 the Smart-seq2 method[55] with some modifications. Briefly, 12 μM $dT_{30}VN$ primer (5'-
565 AAGCAGTGGTATCAACGCAGAGTACT$_{30}$VN-3) were added into microtubes containing cell lysates

566 (final concentration, 1 μM); then, samples were heat-denatured at 70 °C for 3 min, followed by
567 immediate incubation on ice. Next, samples were mixed with a reverse transcription reaction
568 solution containing locked nucleic acid (LNA)-template switching oligo primer (5'-
569 AAGCAGTGGTATCAACGCAGAGTACrGrG+G-3', rG; riboguanosines, +G; LNA-modified guanosine,
570 final concentration of 0.6 μM) and reverse transcriptase (SMARTscribe, Clontech, final
571 concentration of 5 U/μL), and incubated at 42°C for 120 min followed by at 70°C for 10 min to
572 terminate the reaction. The resultant cDNA samples were purified using solid phase reversible
573 immobilization (SPRI) beads (AMPure XP, Beckman Coulter). The purified cDNA samples were
574 amplified by PCR using the IS primer (5'-NH_2-AAGCAGTGGTATCAACGCAGAGT-3', final
575 concentration of 0.24 μM) and Tks Gflex DNA polymerase (Takara Bio, final concentration of 0.025
576 U/μL). The amplified cDNA samples were purified by SPRI beads. The quality and quantity of cDNA
577 sample was confirmed by an Agilent 2100 Bioanalyzer using the High sensitivity DNA kit (Agilent
578 Technology, CA, USA).

579 The cDNA samples were then processed to generate indexed libraries for sequencing using a
580 NEBNext Ultra II DNA Library Prep Kit for Illumina (#E7645, New England Biolabs Inc., Ipswich,
581 MA, USA), according to manufacturer's instructions. Then, libraries were sequenced for 50-bp
582 single-end reads using HiSeq 3000 (Illumina, San Diego, CA, USA). Output fastq files were aligned
583 to the mouse genome (GRCm38/mm10) using STAR aligner[56]. Library size normalization was
584 performed using R (v.4.1.0) by calculating transcripts per million (TPM). Genes with <5 TPM in all

585 samples were excluded from the analysis. We selected 22 genes for neuronal cluster-mediated social
586 behavior in the MPOA based on previous reports[21]. However, *Oprd1* was excluded because of its low
587 expression. Heatmaps were drawn using gplots (v.3.1.1). Differentially expressed genes (DEGs)
588 between virgin, FGE, and paternal mice were analyzed using DESeq2 (v.1.32.0). Genes with a false
589 discovery rate-adjusted $p \leq 0.05$ and a $\log_2$ fold change ≥ 2 in either direction were considered DEGs.
590

591 **Statistical analysis**

592 Group means were compared by Fisher's exact test, the two-tailed t-test, one-way or two-way
593 repeated measures ANOVA followed by a post hoc test as indicated. All statistical tests were two-
594 tailed and conducted with GraphPad Prism software 6 and 9 (GraphPad Software, Inc., La Jolla, CA,
595 USA). A P-value < 0.05 was deemed statistically significant. Statical data was written in the figure
596 legends and Table S7.
597

598 **Data availability**

599 All data that support the findings presented in this study are available from the corresponding
600 author upon request. The raw sequences have been deposited in the DNA Data Bank of Japan
601 (DDBJ) under the DDBJ BioProject umbrella with accession number PRJDB8470, and to the DDBJ
602 Read Archive DRA008585 (BioSample ID: SAMD00175991- SAMD00176002).
603

604 **Lead contact**

605 Further information and requests for resources and reagents should be directed to and will be

606 fulfilled by the lead contact, Taiju Amano (tamano@pharm.hokudai.ac.jp).

607

608 **Figure Legends**

609 Figure 1 The medial amygdala sends projections to the cMPOA

610 (A) Medial amygdala in the parasagittal section. HC; hippocampus, cp; cerebral peduncle, opt; optic

611 tract, EA; extended amygdala, AHi; amygdalohippocampal area, MeP; medial amygdaloid nucleus,

612 posterior part, MeA; medial amygdaloid nucleus, anterior part, LOT; nucleus of the lateral olfactory

613 tract, AA; anterior amygdaloid area.

614 (B) Representative images of the Me stained with anti-Cart visualized with Alexa 488 and BDA

615 visualized with Alexa 568-conjugated streptavidin (magenta). Scale bar = 200 μm.

616 (C) Representative images of the Me injected with the tracer BDA in the MPOA. Parasagittal

617 sections are shown from lateral to medial. Fixed sections were visualized with Alexa 568-conjugated

618 streptavidin (magenta). In parallel, fixed sectioned were immunostained with anti-NPI and

619 visualized with Alexa 488 (green). Main targeted area as the cMPOA (right, lateral 0.5 mm) was

620 represented as the area of yellow line by reference to our previous study[11]. Scale bar = 200 μm.

621 (D) left, summary of experimental procedure. middle, RNA-seq identification of candidate gene

622 expressed in the cMPOA neurons. Heatmap showing a *z*-scored TPM of selected genes for neuronal

623 cluster-mediated social behavior in the MPOA[21]. n = 4 (virgin), 4 (FGE), and 4 (paternal). right,

624 Social experiences of virgin, FGE, and paternal group mice.

625 (E) Representative images of the MPOA. *Galanin* mRNA Alexa 647 -conjugated hairpin DNA (#S23)

626 (magenta), streptavidin conjugated with FITC (green) and DAPI (blue). (e1-e3) magnified images

627 corresponding area in (e), Scale bar = 200 μm for (e, left) and 20 μm for (e1-e3)

628 (F) Representative images of cMPOA neurons after whole-cell patch-clamp recording. Biocytin was

629 infused from recording pipette. Fixed sections visualized with Alexa 488-conjugated streptavidin

630 (green) and *in situ* HCR for *Galanin* mRNA Alexa 647 -conjugated hairpin DNA (#S23) (magenta).

631 Scale bar = 20 μm.

632 (G) Ratio of *Galanin* positive cMPOA neurons targeted for whole-cell patch-clamp recording.

633 (H) Fixed sections were immunostained with anti-NPI visualized with a secondary antibody

634 conjugated to Alexa 488 (green) and immunostained with anti-ERα visualized with a secondary

635 antibody conjugated to Alexa 568 (magenta). Scale bar = 300 μm.

636 (I) Fixed sections were visualized with *in situ* HCR for *Galanin* mRNA Alexa 647 -conjugated hairpin

637 DNA (#S23) (magenta), immunostained with anti-ERα visualized with a secondary antibody

638 conjugated to Alexa 488 (green), and DAPI (blue). Scale bar = 200 μm. f, fornix, ac, anterior

639 commissure.

640 (J) Representative images of cMPOA neurons after whole-cell patch-clamp recording. Biocytin was

641 infused from recording pipette. Fixed sections visualized with Alexa 568-conjugated streptavidin

642 (magenta) and immunostained with anti-ERα and secondary antibody conjugated to Alexa 488

643 (green). Scale bar = 20 μm.

644 (K) Ratio of ERα positive cMPOA neurons targeted for whole-cell patch-clamp recording.

645 (L) Schematic image of the recording and stimulating electrodes on a parasagittal section including

646 the cMPOA. BSTv; bed nucleus of the stria terminalis, ventral part,

647 (M) Input–output curves of stimulus-evoked IPSPs from the *Galanin* positive cMPOA of virgin mice

648 (n = 12 cells; 7 animals) and FGE mice (n = 7 cells; 5 animals). Values are presented as the mean ±

649 standard error. (bottom) Representative traces used to construct input–output curves (40, 80, 120,

650 160, and 200 μA stimuli). Two-way RM ANOVA, $F(1, 17) = 4.964$, $P = 0.0397$ followed by Holm-

651 Sidak post hoc test, *$P < 0.05$, **$P < 0.01$ vs. virgin group.

652 (N) Input–output curves of stimulus-evoked IPSPs from the cMPOA of virgin mice (n = 11 cells; 4

653 animals) and paternal mice (n = 11 cells; 4 animals). Values are presented as the mean ± standard

654 error. (bottom) Representative traces used to construct input–output curves (25, 75, 125, 175 and

655 225 μA stimuli, performed in a different setup and at different stimulation intensity ranges from

656 Figure 1E, 1G and 1H). Two-way RM ANOVA, $F(1, 20) = 10.72$, $P = 0.0038$ followed by Holm-Sidak

657 post hoc test, ***$P < 0.001$, ****$P < 0.0001$ vs. virgin group.

658 (O) Input–output curves of stimulus-evoked IPSPs from paternal mice recorded without (n = 7 cells;

659 2 animals) or with GDPβS (1 mM) in the pipette solution (n = 16 cells; 4 animals). Values are

660 presented as the mean ± standard error. (bottom) Representative traces used to construct

661 input–output curves (40, 80, 120, 160, and 200 μA stimuli). Two-way RM ANOVA, $F(1, 21) = 6.212$,

662 $P = 0.0211$ followed by Holm-Sidak post hoc test, *$P < 0.05$, **$P < 0.01$ vs. paternal group without

663 GDPβS.

664 (P) Input–output curves of stimulus-evoked EPSPs from the cMPOA of virgin mice (n = 21 cells; 3

665 animals) and paternal mice (n = 14 cells; 3 animals). Values are presented as mean ± standard error.

666 (bottom) Representative traces used to construct input–output curves (40, 80, 120, 160, and 200 μA

667 stimuli). Two-way RM ANOVA, $F(1, 33) = 0.7974$, $P > 0.05$.

668

669 Figure 2 Cre-positive neuron in the medial amygdala of Cartpt-Cre mice project to cMPOA neuron

670 (A) Representative images of the MePD in Cartpt-Cre × Ai9 reporter mice. Among MePD neurons

671 immunostained with anti-NeuN antibody visualized with a secondary antibody conjugated to Alexa

672 647 (blue), 21.2% Cartpt neurons (magenta) were tdTomato positive (1 male, 1 female). Scale bar =

673 300 μm. opt; optic tract, LV; lateral ventricle, AHi; amygdalohippocampal area, MePD; posterior-

674 dorsal medial amygdala, MePV; posterior-ventral medial amygdala

675 (B) AAV5-EF1α-DIO-eYFP or AAV5-EF1α-DIO-ChR2-eYFP was injected into the Me of Cartpt-Cre

676 mice. After the expression of eYFP with/without ChR2, whole-cell patch clamp recordings were

677 performed from cMPOA neuron in parasagittal sections of virgin and FGE mouse brain.

678 (C, D) Representative images of eYFP emission from Me (C) and MPOA (D). Me^{Cartpt} neurons sent

679 projection fibers into the MPOA. Scale bar = 200 μm.

680 (E) (left)Schematic image of the recording electrodes on a parasagittal section including the cMPOA.

681 Input fiber from Me^{Cartpt} expressed ChR2 were stimulated by blue light application. BSTv; bed

682 nucleus of the stria terminalis, ventral part, (right) Diagram of dominant responses of IPSC and

683 EPSC with opposite current direction as that of GABAergic and glutamatergic ionotropic receptors.

684 (F) Representative traces of blue light-evoked IPSCs and EPSCs in IPSC- and EPSC-dominant

685 cMPOA neurons. When Me^{Cartpt} neurons were injected with control AAV virus, no responses to

686 optical activation were observed in cMPOA neurons.

687 (G) Relative frequencies of excitatory- and inhibitory-dominant cMPOA neurons in virgin mice (n =

688 12 cells; 4 animals), FGE mice (n = 14 cells; 3 animals), and FGE mice with GDPβS (1 mM) in the

689 pipette solution (n = 9 cells; 2 animals). A significant difference in the ratio of excitatory- to

690 inhibitory-dominant cMPOA neurons between virgin and FGE group mice was observed (Fisher's

691 exact probability test, **P = 0.0048). A significant difference in the ratio of excitatory- and

692 inhibitory-dominant cMPOA neurons between FGE mice and FGE mice with GDPβS (1 mM) in the

693 pipette solution (FGE + GDPβS group) was also observed (Fisher's exact probability test, #P =

694 0.0131).

695

696 Figure 3 The modulation of Me inputs into the cMPOA

697 (A) AAV10-EF1α-DIO-vLWO-eGFP or AAV10-EF1α-DIO-eYFP were injected into the Me of Cartpt-

698 Cre mice and whole-cell recordings were obtained from fluorescent-labeled Me neurons.

699 (B) Representative resting membrane potential traces recorded from a Me^{Cartpt} neuron expressing

700 vLWO. Green light was applied for 20 s (green bar).

701 (C) Effects of green light application on the resting membrane potential in the Me^{Cartpt} neurons

702 expressing vLWO. The data are shown as the averaged potentials between −6 s and −1 s before the

703 onset of green light application (pre-green light) and between 5 s and 10 s after the onset of green

704 light application (green light). Lines represent the data obtained from individual neurons (n = 5),

705 and bars represent the averaged data obtained from five neurons. **P = 0.0017, two-tailed paired t-

706 test (t = 7.466, df = 4), compared with pre-green light application.

707 (D) Representative resting membrane potential traces recorded from a Me^{Cartpt} neuron expressing

708 control eYFP. Green light was applied for 20 s (green bar). Five animals were excluded due to

709 exclusion criteria.

710 (E) Effects of green light application on the resting membrane potential in the Me^{Cartpt} neurons

711 expressing control eYFP. Lines represent the data obtained from individual neurons (n = 10), and

712 bars represent the averaged data obtained from nine neurons. P = 0.6308, two-tailed paired t-test

713 (t=0.4975 df=9), compared with pre-green light application.

714 (F) AAV5-DIO-ChR2(H134R)-mCherry and AAV10-EF1α-DIO-vLWO-eGFP-5HT1A was injected into

715 the Me of Cartpt-Cre mice and whole-cell recordings were obtained from cMPOA neurons.

716 (G) Representative images of the Me expressing eGFP and mCherry. Scale bar = 200 μm.

717 (H) Representative traces of blue light-evoked IPSCs in the cMPOA neurons. Red bar indicates red

718 light application (2 s).

719 (I) Effects of red-light application on the blue light-evoked postsynaptic currents in the cMPOA

720 neurons. Lines represent the data obtained from individual neurons (n = 4), and bars represent the

721 averaged data obtained. ***P = 0.0007, two-tailed paired t-test (t=14.25 df=3), compared with pre-

722 red light application.

723 (J) AAV10-EF1α-DIO-vLWO-eGFP was injected into the Me of Cartpt-Cre mice and whole-cell

724 recordings were obtained from cMPOA neurons.

725 (K) Representative trace of green light-induced modulation of sIPSCs in the cMPOA neurons. Data

726 were obtained in the presence of CNQX (20 μM) and MK-801 (20 μM). Green light was applied for

727 20 s.

728 (L) Effects of green light application on the frequency of sIPSC in the cMPOA neurons. Lines

729 represent the data obtained from individual neurons (n = 25), and bars represent the averaged data.

730 Repeated measures ANOVA, F (1.468, 35.23) = 3.962, P = 0.0396, followed by Dunnett's multiple

731 comparisons post hoc test *P = 0.0332 compared with pre-green light application. One data showed

732 large sIPSC frequency. It was judged as an outlier in Grubbs' test. Without this data point, the same

733 repeated measure ANOVA analysis resulted in F (1.733, 39.87) = 4.149, P=0.0279, indicating that

734 the conclusion remains when leaving out this outlier.

735 (M) Representative trace of sIPSCs in the cMPOA neurons in the presence of TTX (1 μM).

736 (N) Application of TTX blocked the green light induced changes of IPSCs frequency. Lines represent

737 the data obtained from individual neurons (n = 12), and bars represent the averaged data. Repeated

738 measures ANOVA, F (1.236, 13.60) = 0.2769, P = 0.6561.

739

740 Figure 4 Optogenetic manipulation of the Me^{Cartpt}–cMPOA input suppressed infanticidal behavior of

741 virgin male mice

742 (A, B) Representative images of c-Fos induction in the Me following pup exposure (A) and in the

743 control Me (B). Fixed sections were stained with anti-c-Fos and visualized with Alexa 647 (magenta).

744 eYFP was expressed by injection of AAV10-EF1α-DIO-eYFP. Scale bar = 200 μm for 10× images.

745 Scale bar = 50 μm for 60× images.

746 (C) Percentage of c-Fos-positive Me^{Cartpt} neurons out of all eYFP-positive Me^{Cartpt} neurons following

747 pup exposure. A pup kept in a metal net to avoid biting attacks was placed in the test cage for 30

748 min (n = 3). An empty metal net was added as a control (n = 3). ****P < 0.0001, two-tailed unpaired

749 t-test (t = 23.41, df = 4).

750 (D) AAV10-EF1α-DIO-vLWO-eGFP-5HT1A or AAV10-EF1α-DIO-eYFP was injected into the Me of

751 Cartpt-Cre mice. Five weeks later, glass fibers were implanted above the cMPOA for pathway

752 stimulation. During the behavioral test, 532 nm green light was applied following a repeated

753 protocol of 20 s on and 10 s off.

754 (E) Latencies to first sniffing were compared between vLWO and control group mice. Two-way RM

755 ANOVA, F (1, 16) = 1.642, P = 0.2183.

756 (F, G) Relative frequencies of paternal/infanticidal behaviors toward pups during manipulation of

757 the Me^{Cartpt}-to-cMPOA input by vLWO activation. Significant difference in the ratio showing

758 infanticidal behavior between mice expressing vLWO-eGFP (n = 8, F) or eYFP only (n = 10, G) *P =

759 0.0229, **P = 0.0065, Fisher's exact probability test. Eight animals of vLWO group were excluded

760 due to exclusion criteria.

761

762 Figure 5

763 Optogenetic inhibition of the Me–cMPOA input in vGAT-IRES-Cre mice suppressed infanticidal

764 behavior of virgin male mice

765 (A) AAV10- EF1α-DIO-vLWO-eGFP-5HT1A or AAV10-EF1α-DIO-eYFP was injected into the Me of

766 vGAT-IRES-Cre mice. Five weeks later, glass fibers were implanted above the cMPOA. During the

767 behavioral test, 532 nm green light was repeatedly applied at 20 s on and 10 s off.

768 (B) Representative images of eYFP emission from the MPOA of vGAT-IRES-Cre mice (green).

769 Sections including the Me were immunostained with anti-NPI and visualized with a secondary

770 antibody conjugated to Alexa 594 (magenta).

771 (C) Representative images of eYFP expressed in the Me of vGAT-IRES-Cre mice (green). Sections

772 were immunostained with anti-Cart and visualized with a secondary antibody conjugated to Alexa

773 594 (magenta). All scale bar = 200 μm.

774 (D, E) Relative frequencies of paternal/infanticidal behaviors during vLWO activation at the Me^{vGAT}

775 input into cMPOA. Significant difference in the ratio of mice showing infanticide between vLWO (n

776 = 7, D) and control (n = 10, E) groups (Fisher's exact probability test, *P = 0.0345).

777

778 Figure 6 Inhibitory synaptic inputs into the BSTrh were potentiated in paternal group mice

779 (A) Whole-cell patch clamp recordings were performed on BSTrh neurons (Rec). To observe the

780 evoked synaptic responses, electrical stimulation was delivered through a stimulating electrode

781 (Stim). rh, rhomboid nucleus; pr, principal nucleus; LV, lateral ventricle; ic, internal capsule; f,

782 fornix; D3V, dorsal third ventricle; GP, globus pallidus; ac, anterior commissure; ST, stria terminalis

783 (B) Input–output curves of stimulus-evoked IPSPs from virgin mice (n = 16 cells; 10 animals),

784 paternal mice (n = 17 cells; 11 animals), and FGE mice (n = 10 cells; 5 animals). Values are

785 presented as the mean ± standard error. (inset) Representative traces used to construct

786 input–output curves (50, 100, 150, and 200 μA stimuli). Two-way RM ANOVA, F (2, 40) = 5.416, P =

787 0.0083, followed by Holm-Sidak post hoc test, *P < 0.05, **P < 0.01 vs. virgin group.

788 (C) Input–output curves of stimulus-evoked EPSPs from virgin mice (n = 9 cells; 6 animals),

789 paternal mice (n = 15 cells; 6 animals), and FGE mice (n = 6 cells; 3 animals). Values are presented

790 as the mean ± standard error. (inset) Representative traces used to construct input–output curves

791 (25 and 100 μA stimuli). Two-way RM ANOVA, F (2, 27) = 0.4838, P > 0.05.

792 (D) Photographs of the MPOA from sham-operated and NMDA-lesioned mice. Sections were

793 immunostained with anti-NeuN and visualized with DAB. Arrowhead indicates the ventral edge of

794 lesioned area. Scale bar = 500 μm.

795 (E) Input–output curves of stimulus-evoked IPSPs from paternal sham-operated mice (sham; n = 26

796 from 7 mice, NMDA; n = 15 from 6 mice). Values are presented as the mean ± standard error. (inset)

797 Representative traces used to construct input–output curves (25, 75, 125, and 175 μA stimuli). Two-

798 way RM ANOVA, $F(1, 29) = 10.30$, $P = 0.0032$ followed by Holm-Sidak post hoc test, *$P < 0.05$, **$P <$

799 0.01, ***$P < 0.001$ vs. virgin group.

800 (F) Input–output curves of stimulus-evoked IPSPs from sham-operated virgin mice (sham; n = 7

801 cells; 4 animals) and cMPOA-lesioned virgin mice (NMDA; n = 9 cells; 4 animals). Values are

802 presented as the mean ± standard error. (inset) Representative traces used to construct

803 input–output curves (25, 75, 125, and 175 μA stimuli). Two-way RM ANOVA, $F(1, 14) = 0.9177$, $P >$

804 0.05.

805 (G) Input–output curves of stimulus-evoked IPSPs from virgin mice (n = 10 cells; 4 animals) and

806 paternal mice (n = 9 cells; 4 animals) recorded with GDPβS (1 mM) in the pipette solution. Values

807 are presented as mean ± standard error. (inset) Representative traces used to construct

808 input–output curves (50, 100, 150, and 200 μA stimuli). Two-way RM ANOVA, $F(1, 17) = 0.1907$, P

809 > 0.05.

810 (H) Input–output curves of stimulus-evoked EPSPs from virgin mice (n = 9 cells; 5 animals) and

811 paternal mice (n = 10 cells; 4 animals) recorded with GDPβS (1 mM) in the pipette solution. Values

812 are presented as mean ± standard error. (inset) Representative traces used to construct

813 input–output curves (25, 75 and 125 μA stimuli). Two-way RM ANOVA, $F(1, 17) = 0.4811$, $P > 0.05$.

814 (I) (top) Paired-pulse ratio of eEPSCs (inter-stimulation interval = 50 ms) from virgin mice (n = 6

815 cells; 5 animals) and paternal mice (n = 7 cells; 6 animals). Two-tailed unpaired t-test: $P > 0.05$.

816 (bottom) Paired-pulse ratio of eIPSCs (inter-stimulation interval = 100 ms) from virgin mice (n = 10

817 cells; 9 animals) and paternal mice (n = 15 cells; 10 animals). Two-tailed unpaired t-test, $P > 0.05$.

818

819 **References**

820 1. Elwood, R.W. (1977). Changes in Responses of Male and Female Gerbils (Meriones-
821 Unguiculatus) Towards Test Pups during Pregnancy of Female. Anim Behav *25*, 46-51. Doi
822 10.1016/0003-3472(77)90066-5.
823 2. Hausfater, G., and Hrdy, S.B. (1984). Infanticide: Comparative and Evolutionary
824 Perspectives (Routledge).
825 3. Hrdy, S.B. (1974). Male-Male Competition and Infanticide among Langurs (Presbytis-
826 Entellus) of Abu, Rajasthan. Folia Primatol *22*, 19-58.
827 4. van Schaik, C.P., and Janson, C.P. (2000). Infanticide by Males and its Implications
828 (Cambridge University Press).
829 5. vom Saal, F.S., and Howard, L.S. (1982). The regulation of infanticide and parental
830 behavior: implications for reproductive success in male mice. Science *215*, 1270-1272.
831 6. Palombit, R.A. (2015). Infanticide as Sexual Conflict: Coevolution of Male Strategies and
832 Female Counterstrategies. Csh Perspect Biol *7*. 10.1101/cshperspect.a017640.
833 7. vom Saal, F.S. (1985). Time-contingent change in infanticide and parental behavior induced
834 by ejaculation in male mice. Physiol Behav *34*, 7-15.
835 8. Tachikawa, K.S., Yoshihara, Y., and Kuroda, K.O. (2013). Behavioral transition from attack
836 to parenting in male mice: a crucial role of the vomeronasal system. The Journal of
837 neuroscience : the official journal of the Society for Neuroscience *33*, 5120-5126.
838 10.1523/JNEUROSCI.2364-12.2013.
839 9. Numan, M. (1974). Medial preoptic area and maternal behavior in the female rat. J Comp
840 Physiol Psychol *87*, 746-759.
841 10. Tsuneoka, Y., Maruyama, T., Yoshida, S., Nishimori, K., Kato, T., Numan, M., and Kuroda,
842 K.O. (2013). Functional, anatomical, and neurochemical differentiation of medial preoptic
843 area subregions in relation to maternal behavior in the mouse. The Journal of comparative

844 neurology *521*, 1633-1663. 10.1002/cne.23251.
845 11. Tsuneoka, Y., Tokita, K., Yoshihara, C., Amano, T., Esposito, G., Huang, A.J., Yu, L.M.,
846 Odaka, Y., Shinozuka, K., McHugh, T.J., and Kuroda, K.O. (2015). Distinct preoptic-BST
847 nuclei dissociate paternal and infanticidal behavior in mice. The EMBO journal *34*, 2652-
848 2670. 10.15252/embj.201591942.
849 12. Wu, Z., Autry, A.E., Bergan, J.F., Watabe-Uchida, M., and Dulac, C.G. (2014). Galanin
850 neurons in the medial preoptic area govern parental behaviour. Nature *509*, 325-330.
851 10.1038/nature13307.
852 13. Keshavarzi, S., Sullivan, R.K., Ianno, D.J., and Sah, P. (2014). Functional properties and
853 projections of neurons in the medial amygdala. The Journal of neuroscience : the official
854 journal of the Society for Neuroscience *34*, 8699-8715. 10.1523/JNEUROSCI.1176-14.2014.
855 14. Kohl, J., Babayan, B.M., Rubinstein, N.D., Autry, A.E., Marin-Rodriguez, B., Kapoor, V.,
856 Miyamishi, K., Zweifel, L.S., Luo, L., Uchida, N., and Dulac, C. (2018). Functional
857 circuit architecture underlying parental behaviour. Nature *556*, 326-331. 10.1038/s41586-
858 018-0027-0.
859 15. Simerly, R.B., and Swanson, L.W. (1986). The organization of neural inputs to the medial
860 preoptic nucleus of the rat. The Journal of comparative neurology *246*, 312-342.
861 10.1002/cne.902460304.
862 16. Mei, L., Yan, R., Yin, L., Sullivan, R.M., and Lin, D. (2023). Antagonistic circuits
863 mediating infanticide and maternal care in female mice. Nature. 10.1038/s41586-023-06147-9.
864 17. Chen, P.B., Hu, R.K., Wu, Y.E., Pan, L., Huang, S., Micevych, P.E., and Hong, W. (2019).
865 Sexually Dimorphic Control of Parenting Behavior by the Medial Amygdala. Cell *176*, 1206-
866 1221.e1218. 10.1016/j.cell.2019.01.024.
867 18. Broberger, C. (1999). Hypothalamic cocaine- and amphetamine-regulated transcript (CART)
868 neurons: histochemical relationship to thyrotropin-releasing hormone, melanin-
869 concentrating hormone, orexin/hypocretin and neuropeptide Y. Brain Res *848*, 101-113.
870 19. Wu, Y.E., Pan, L., Zuo, Y., Li, X., and Hong, W. (2017). Detecting Activated Cell
871 Populations Using Single-Cell RNA-Seq. Neuron *96*, 313-329 e316.
872 10.1016/j.neuron.2017.09.026.
873 20. Sato, K., Hamasaki, Y., Fukui, K., Ito, K., Miyamichi, K., Minami, M., and Amano, T.
874 (2020). Amygdalohippocampal Area Neurons That Project to the Preoptic Area Mediate Infant-
875 Directed Attack in Male Mice. The Journal of neuroscience : the official journal of the
876 Society for Neuroscience *40*, 3981-3994. 10.1523/JNEUROSCI.0438-19.2020.
877 21. Moffitt, J.R., Bambah-Mukku, D., Eichhorn, S.W., Vaughn, E., Shekhar, K., Perez, J.D.,
878 Rubinstein, N.D., Hao, J., Regev, A., Dulac, C., and Zhuang, X. (2018). Molecular, spatial,
879 and functional single-cell profiling of the hypothalamic preoptic region. Science *362*.
880 10.1126/science.aau5324.
881 22. Fang, Y.Y., Yamaguchi, T., Song, S.C., Tritsch, N.X., and Lin, D. (2018). A Hypothalamic

882 Midbrain Pathway Essential for Driving Maternal Behaviors. Neuron *98*, 192-207 e110.
883 10.1016/j.neuron.2018.02.019.
884 23. Wei, Y.C., Wang, S.R., Jiao, Z.L., Zhang, W., Lin, J.K., Li, X.Y., Li, S.S., Zhang, X.,
885 and Xu, X.H. (2018). Medial preoptic area in mice is capable of mediating sexually
886 dimorphic behaviors regardless of gender. Nat Commun *9*, 279. 10.1038/s41467-017-02648-0.
887 24. Masseck, O.A., Spoida, K., Dalkara, D., Maejima, T., Rubelowski, J.M., Wallhorn, L.,
888 Deneris, E.S., and Herlitze, S. (2014). Vertebrate cone opsins enable sustained and highly
889 sensitive rapid control of Gi/o signaling in anxiety circuitry. Neuron *81*, 1263-1273.
890 10.1016/j.neuron.2014.01.041.
891 25. Soya, S., Takahashi, T.M., McHugh, T.J., Maejima, T., Herlitze, S., Abe, M., Sakimura, K.,
892 and Sakurai, T. (2017). Orexin modulates behavioral fear expression through the locus
893 coeruleus. Nat Commun *8*, 1606. 10.1038/s41467-017-01782-z.
894 26. Amano, T., Shindo, S., Yoshihara, C., Tsuneoka, Y., Uki, H., Minami, M., and Kuroda, K.O.
895 (2017). Development-dependent behavioral change toward pups and synaptic transmission in
896 the rhomboid nucleus of the bed nucleus of the stria terminalis. Behav Brain Res *325*, 131-
897 137. 10.1016/j.bbr.2016.10.029.
898 27. Elwood, R.W. (1985). Inhibition of Infanticide and Onset of Paternal Care in Male-Mice
899 (Mus-Musculus). J Comp Psychol *99*, 457-467. Doi 10.1037//0735-7036.99.4.457.
900 28. Inada, K., Hagihara, M., Tsujimoto, K., Abe, T., Konno, A., Hirai, H., Kiyonari, H., and
901 Miyamichi, K. (2022). Plasticity of neural connections underlying oxytocin-mediated
902 parental behaviors of male mice. Neuron. 10.1016/j.neuron.2022.03.033.
903 29. Hong, W., Kim, D.W., and Anderson, D.J. (2014). Antagonistic control of social versus
904 repetitive self-grooming behaviors by separable amygdala neuronal subsets. Cell *158*, 1348-
905 1361. 10.1016/j.cell.2014.07.049.
906 30. Kondo, Y. (1992). Lesions of the medial amygdala produce severe impairment of copulatory
907 behavior in sexually inexperienced male rats. Physiol Behav *51*, 939-943.
908 31. Li, Y., Mathis, A., Grewe, B.F., Osterhout, J.A., Ahanonu, B., Schnitzer, M.J., Murthy,
909 V.N., and Dulac, C. (2017). Neuronal Representation of Social Information in the Medial
910 Amygdala of Awake Behaving Mice. Cell *171*, 1176-1190 e1117. 10.1016/j.cell.2017.10.015.
911 32. Sano, K., Nakata, M., Musatov, S., Morishita, M., Sakamoto, T., Tsukahara, S., and Ogawa,
912 S. (2016). Pubertal activation of estrogen receptor alpha in the medial amygdala is
913 essential for the full expression of male social behavior in mice. Proc Natl Acad Sci U S
914 A *113*, 7632-7637. 10.1073/pnas.1524907113.
915 33. Sano, K., Tsuda, M.C., Musatov, S., Sakamoto, T., and Ogawa, S. (2013). Differential
916 effects of site-specific knockdown of estrogen receptor alpha in the medial amygdala,
917 medial pre-optic area, and ventromedial nucleus of the hypothalamus on sexual and
918 aggressive behavior of male mice. Eur J Neurosci *37*, 1308-1319. 10.1111/ejn.12131.
919 34. Dominguez, J., Riolo, J.V., Xu, Z., and Hull, E.M. (2001). Regulation by the medial

920 amygdala of copulation and medial preoptic dopamine release. The Journal of neuroscience :
921 the official journal of the Society for Neuroscience *21*, 349-355.
922 35. Kondo, Y., and Arai, Y. (1995). Functional association between the medial amygdala and the
923 medial preoptic area in regulation of mating behavior in the male rat. Physiol Behav *57*,
924 69-73.
925 36. Choi, G.B., Dong, H.W., Murphy, A.J., Valenzuela, D.M., Yancopoulos, G.D., Swanson, L.W.,
926 and Anderson, D.J. (2005). Lhx6 delineates a pathway mediating innate reproductive
927 behaviors from the amygdala to the hypothalamus. Neuron *46*, 647-660.
928 10.1016/j.neuron.2005.04.011.
929 37. Pardo-Bellver, C., Cadiz-Moretti, B., Novejarque, A., Martinez-Garcia, F., and Lanuza, E.
930 (2012). Differential efferent projections of the anterior, posteroventral, and
931 posterodorsal subdivisions of the medial amygdala in mice. Front Neuroanat *6*, 33.
932 10.3389/fnana.2012.00033.
933 38. Morris, J.A., Jordan, C.L., and Breedlove, S.M. (2008). Sexual dimorphism in neuronal
934 number of the posterodorsal medial amygdala is independent of circulating androgens and
935 regional volume in adult rats. The Journal of comparative neurology *506*, 851-859.
936 10.1002/cne.21536.
937 39. Unger, E.K., Burke, K.J., Jr., Yang, C.F., Bender, K.J., Fuller, P.M., and Shah, N.M.
938 (2015). Medial amygdalar aromatase neurons regulate aggression in both sexes. Cell Rep *10*,
939 453-462. 10.1016/j.celrep.2014.12.040.
940 40. Rogge, G., Jones, D., Hubert, G.W., Lin, Y., and Kuhar, M.J. (2008). CART peptides:
941 regulators of body weight, reward and other functions. Nat Rev Neurosci *9*, 747-758.
942 10.1038/nrn2493.
943 41. Allen, W.E., DeNardo, L.A., Chen, M.Z., Liu, C.D., Loh, K.M., Fenno, L.E., Ramakrishnan,
944 C., Deisseroth, K., and Luo, L. (2017). Thirst-associated preoptic neurons encode an
945 aversive motivational drive. Science *357*, 1149-1155. 10.1126/science.aan6747.
946 42. Chung, S., Weber, F., Zhong, P., Tan, C.L., Nguyen, T.N., Beier, K.T., Hormann, N., Chang,
947 W.C., Zhang, Z., Do, J.P., et al. (2017). Identification of preoptic sleep neurons using
948 retrograde labelling and gene profiling. Nature *545*, 477-481. 10.1038/nature22350.
949 43. McHenry, J.A., Otis, J.M., Rossi, M.A., Robinson, J.E., Kosyk, O., Miller, N.W.,
950 McElligott, Z.A., Budygin, E.A., Rubinow, D.R., and Stuber, G.D. (2017). Hormonal gain
951 control of a medial preoptic area social reward circuit. Nat Neurosci *20*, 449-458.
952 10.1038/nn.4487.
953 44. Tan, C.L., Cooke, E.K., Leib, D.E., Lin, Y.C., Daly, G.E., Zimmerman, C.A., and Knight,
954 Z.A. (2016). Warm-Sensitive Neurons that Control Body Temperature. Cell *167*, 47-59 e15.
955 10.1016/j.cell.2016.08.028.
956 45. Fumero, B., Fernandez-Vera, J.R., Gonzalez-Mora, J.L., and Mas, M. (1994). Changes in
957 monoamine turnover in forebrain areas associated with masculine sexual behavior: a

958 microdialysis study. Brain Res *662*, 233-239.
959 46. Nutsch, V.L., Will, R.G., Robison, C.L., Martz, J.R., Tobiansky, D.J., and Dominguez, J.M.
960 (2016). Colocalization of Mating-Induced Fos and D2-Like Dopamine Receptors in the Medial
961 Preoptic Area: Influence of Sexual Experience. Front Behav Neurosci *10*, 75.
962 10.3389/fnbeh.2016.00075.
963 47. Ren, W.J., Centeno, M.V., Berger, S., Wu, Y., Na, X.D., Liu, X.G., Kondapalli, J.,
964 Apkarian, A.V., Martina, M., and Surmeier, D.J. (2016). The indirect pathway of the
965 nucleus accumbens shell amplifies neuropathic pain. Nature Neuroscience *19*, 220-+.
966 10.1038/nn.4199.
967 48. Thompson, D., Martini, L., and Whistler, J.L. (2010). Altered ratio of D1 and D2 dopamine
968 receptors in mouse striatum is associated with behavioral sensitization to cocaine. PLoS
969 One *5*, e11038. 10.1371/journal.pone.0011038.
970 49. Jacob, T.C., Moss, S.J., and Jurd, R. (2008). GABA(A) receptor trafficking and its role in
971 the dynamic modulation of neuronal inhibition. Nat Rev Neurosci *9*, 331-343.
972 10.1038/nrn2370.
973 50. Seelke, A.M.H., Bond, J.M., Simmons, T.C., Joshi, N., Settles, M.L., Stolzenberg, D.,
974 Rhemtulla, M., and Bales, K.L. (2018). Fatherhood alters gene expression within the MPOA.
975 Environ Epigenet *4*, dvy026. 10.1093/eep/dvy026.
976 51. Tsuneoka, Y., Yoshida, S., Takase, K., Oda, S., Kuroda, M., and Funato, H. (2017).
977 Neurotransmitters and neuropeptides in gonadal steroid receptor-expressing cells in medial
978 preoptic area subregions of the male mouse. Sci Rep *7*, 9809. 10.1038/s41598-017-10213-4.
979 52. Kawai, S., Takagi, Y., Kaneko, S., and Kurosawa, T. (2011). Effect of three types of mixed
980 anesthetic agents alternate to ketamine in mice. Exp Anim *60*, 481-487.
981 53. Tsuneoka, Y., Atsumi, Y., Makanae, A., Yashiro, M., and Funato, H. (2022). Fluorescence
982 quenching by high-power LEDs for highly sensitive fluorescence in situ hybridization.
983 Front Mol Neurosci *15*, 976349. 10.3389/fnmol.2022.976349.
984 54. Tsuneoka, Y., and Funato, H. (2020). Modified in situ Hybridization Chain Reaction Using
985 Short Hairpin DNAs. Front Mol Neurosci *13*, 75. 10.3389/fnmol.2020.00075.
986 55. Picelli, S., Faridani, O.R., Bjorklund, A.K., Winberg, G., Sagasser, S., and Sandberg, R.
987 (2014). Full-length RNA-seq from single cells using Smart-seq2. Nat Protoc *9*, 171-181.
988 10.1038/nprot.2014.006.
989 56. Dobin, A., Davis, C.A., Schlesinger, F., Drenkow, J., Zaleski, C., Jha, S., Batut, P.,
990 Chaisson, M., and Gingeras, T.R. (2013). STAR: ultrafast universal RNA-seq aligner.
991 Bioinformatics *29*, 15-21. 10.1093/bioinformatics/bts635.

992

Figure 1

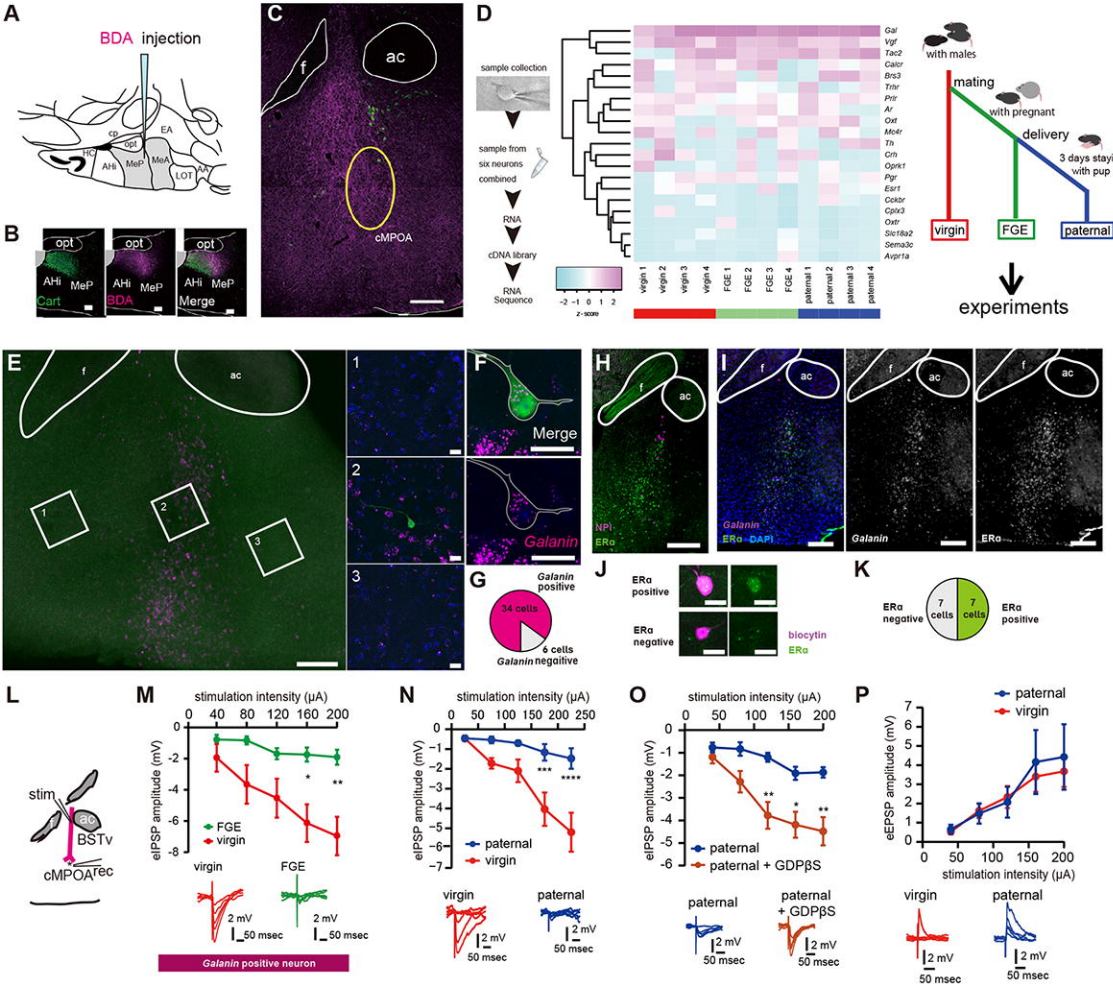
A
BDA injection
cp
opt
EA
HC
AHi
MeP
MeA
LOT
AP
B
opt
AHi
MeP
Cart
BDA
Merge
C
f
ac
cMPOA
D
sample collection
sample from six neurons combined
RNA
cDNA library
RNA Sequence
Z-score
virgin 1
virgin 2
virgin 3
virgin 4
FGE 1
FGE 2
FGE 3
FGE 4
paternal 1
paternal 2
paternal 3
paternal 4
Gal
Vgf
Tac2
Galcr
Brs3
Trhr
Prlr
Ar
Oxt
Mc4r
Th
Crh
Oprk1
Pgr
Esr1
Cckbr
Cplx3
Oxtr
Slc18a2
Sema3c
Avpr1a
with males
mating
with pregnant
delivery
3 days staying with pup
virgin
FGE
paternal
experiments
E
f
ac
1
2
3
F
Merge
Galanin
G
Galanin positive
34 cells
6 cells
Galanin negative
H
f
ac
NPi
ERα
I
f
ac
Galanin
ERα
DAPI
Galanin
ERα
J
ERα positive
ERα negative
biocytin
ERα
K
ERα negative
7 cells
7 cells
ERα positive
L
stim
ac
BSTv
cMPOA
rec
M
stimulation intensity (μA)
0 40 80 120 160 200
eIPSP amplitude (mV)
0 -2 -4 -6 -8
FGE
virgin
virgin
FGE
2 mV
50 msec
Galanin positive neuron
N
stimulation intensity (μA)
0 50 100 150 200 250
eIPSP amplitude (mV)
0 -1 -2 -3 -4 -5 -6 -7
paternal
virgin
virgin
paternal
2 mV
50 msec
O
stimulation intensity (μA)
0 50 100 150 200
eIPSP amplitude (mV)
0 -1 -2 -3 -4 -5 -6
paternal
paternal + GDPβS
paternal
paternal + GDPβS
2 mV
50 msec
P
paternal
virgin
eEPSP amplitude (mV)
0 1 2 3 4 5 6 7
0 50 100 150 200
stimulation intensity (μA)
virgin
paternal
2 mV
50 msec

Figure 2

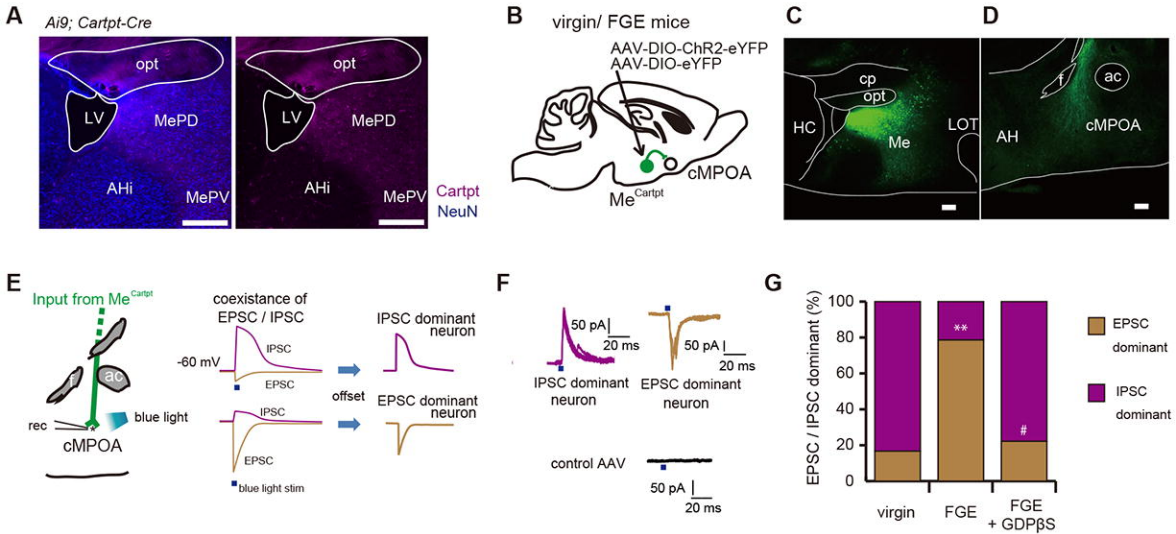
A
Ai9; Cartpt-Cre
opt
LV
MePD
AHi
MePV
Cartpt
NeuN
B
virgin/ FGE mice
AAV-DIO-ChR2-eYFP
AAV-DIO-eYFP
cMPOA
Me Cartpt
C
D
cp
opt
HC
Me
LOT
f
ac
AH
cMPOA
E
Input from Me Cartpt
ac
rec
blue light
cMPOA
coexistance of
EPSC / IPSC
-60 mV
IPSC
EPSC
offset
blue light stim
IPSC dominant
neuron
EPSC dominant
neuron
F
50 pA
20 ms
IPSC dominant
neuron
EPSC dominant
neuron
control AAV
G
EPSC / IPSC dominant (%)
100
80
60
40
20
0
**
#
virgin
FGE
FGE
+ GDPβS
EPSC
dominant
IPSC
dominant

Figure 3

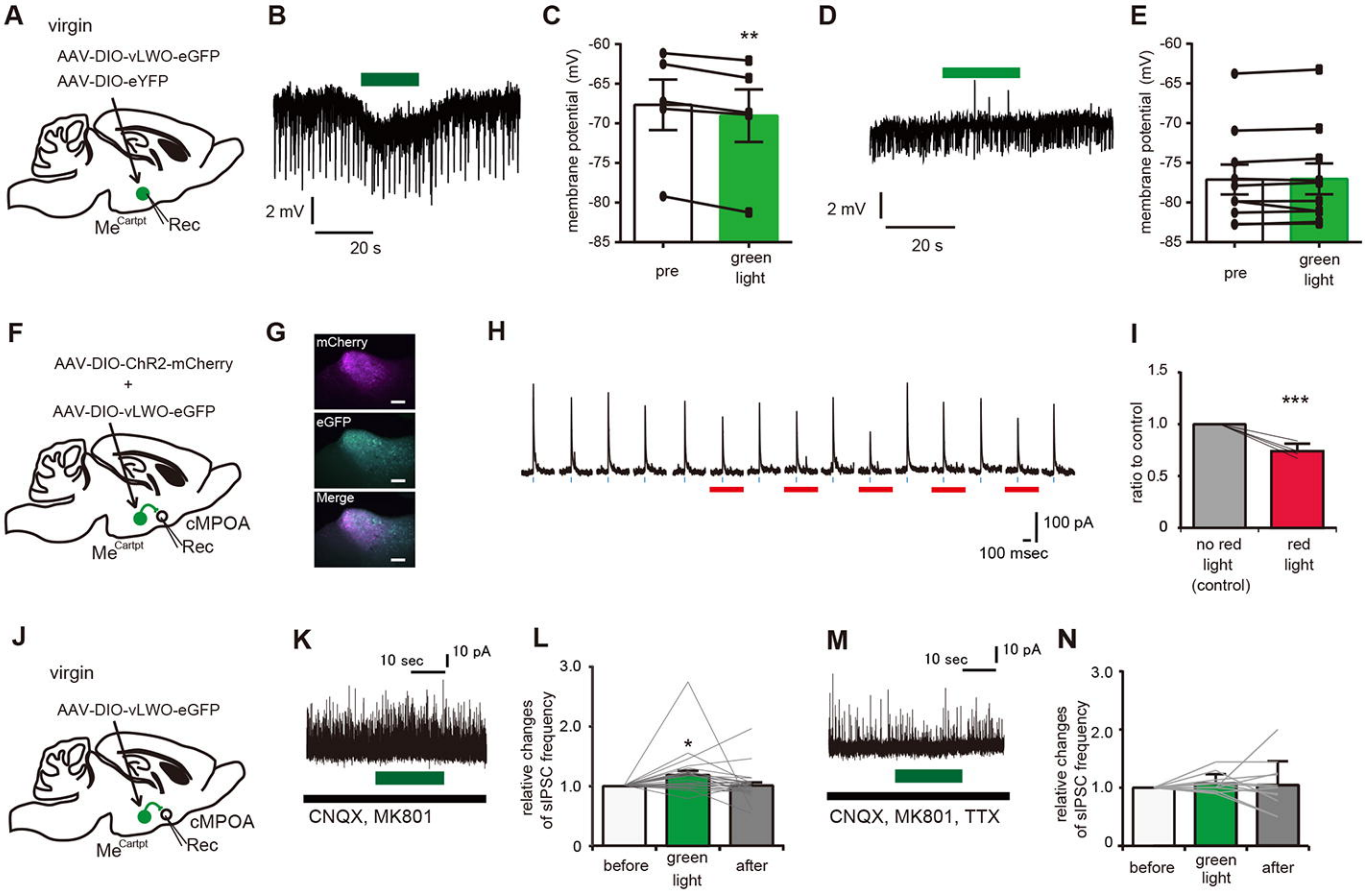
A
virgin
AAV-DIO-vLWO-eGFP
AAV-DIO-eYFP
Me Cartpt
Rec
B
2 mV
20 s
C
**
membrane potential (mV)
-60
-65
-70
-75
-80
-85
pre
green light
D
2 mV
20 s
E
membrane potential (mV)
-60
-65
-70
-75
-80
-85
pre
green light
F
AAV-DIO-ChR2-mCherry
+
AAV-DIO-vLWO-eGFP
cMPOA
Me Cartpt
Rec
G
mCherry
eGFP
Merge
H
100 pA
100 msec
I
***
ratio to control
1.5
1.0
0.5
0
no red light (control)
red light
J
virgin
AAV-DIO-vLWO-eGFP
cMPOA
Me Cartpt
Rec
K
10 sec
10 pA
CNQX, MK801
L
*
relative changes of sIPSC frequency
3.0
2.0
1.0
0
before
green light
after
M
10 sec
10 pA
CNQX, MK801, TTX
N
relative changes of sIPSC frequency
3.0
2.0
1.0
0
before
green light
after

Figure 4

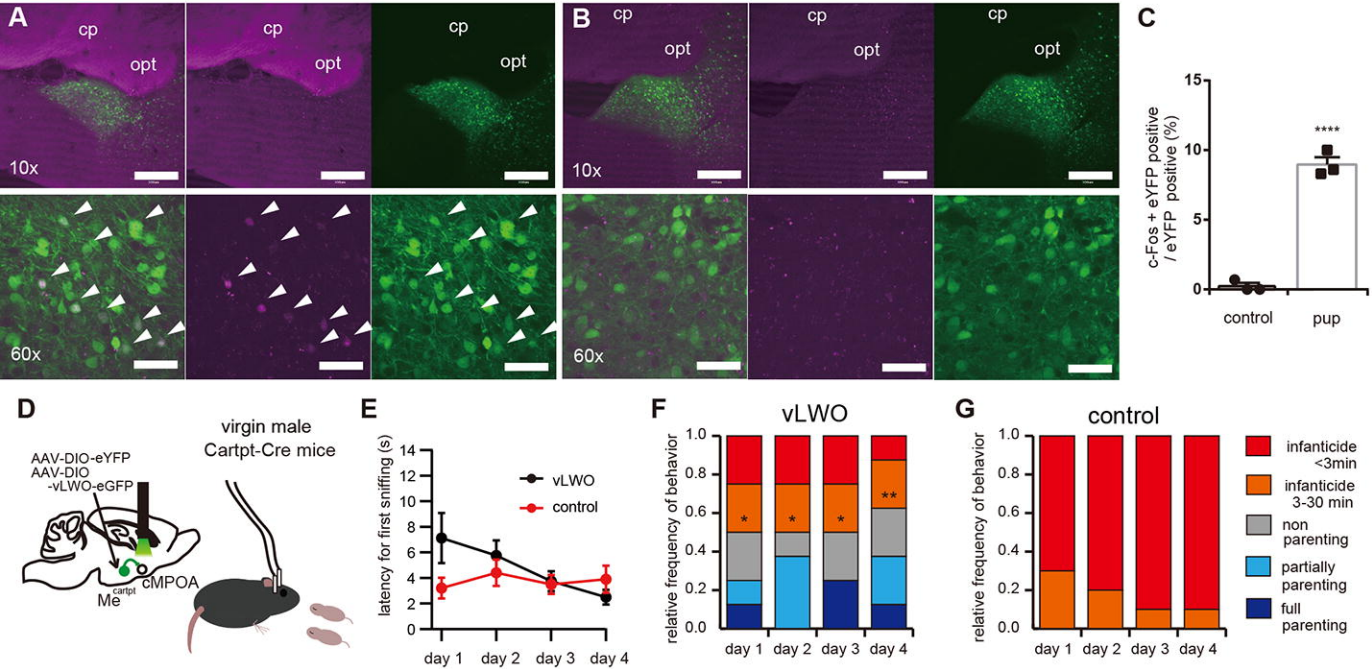
A
cp
opt
10x
60x
B
C
c-Fos + eYFP positive / eYFP positive (%)
****
control
pup
D
AAV-DIO-eYFP
AAV-DIO -vLWO-eGFP
virgin male
Cartpt-Cre mice
cMPOA
Me
cartpt
E
latency for first sniffing (s)
vLWO
control
day 1
day 2
day 3
day 4
F
vLWO
relative frequency of behavior
G
control
infanticide <3min
infanticide 3-30 min
non parenting
partially parenting
full parenting

Figure 5

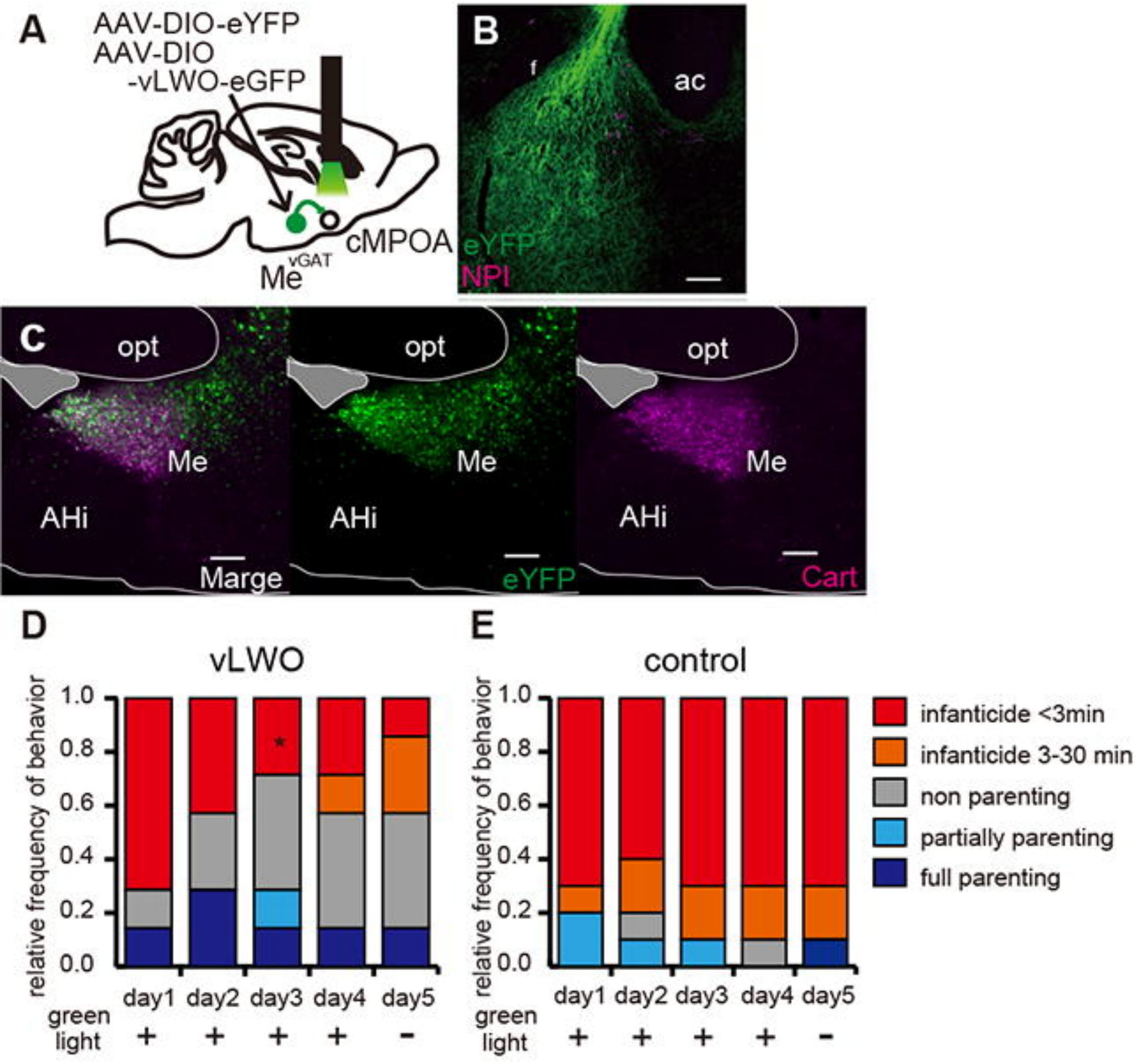
A
AAV-DIO-eYFP
AAV-DIO
-vLWO-eGFP
cMPOA
Me vGAT
B
f
ac
eYFP
NPI
C
opt
Me
AHi
Marge
eYFP
Cart
D
vLWO
relative frequency of behavior
1.0
0.8
0.6
0.4
0.2
0.0
day1 day2 day3 day4 day5
green light
+ + + + -
E
control
infanticide <3min
infanticide 3-30 min
non parenting
partially parenting
full parenting

Figure 6

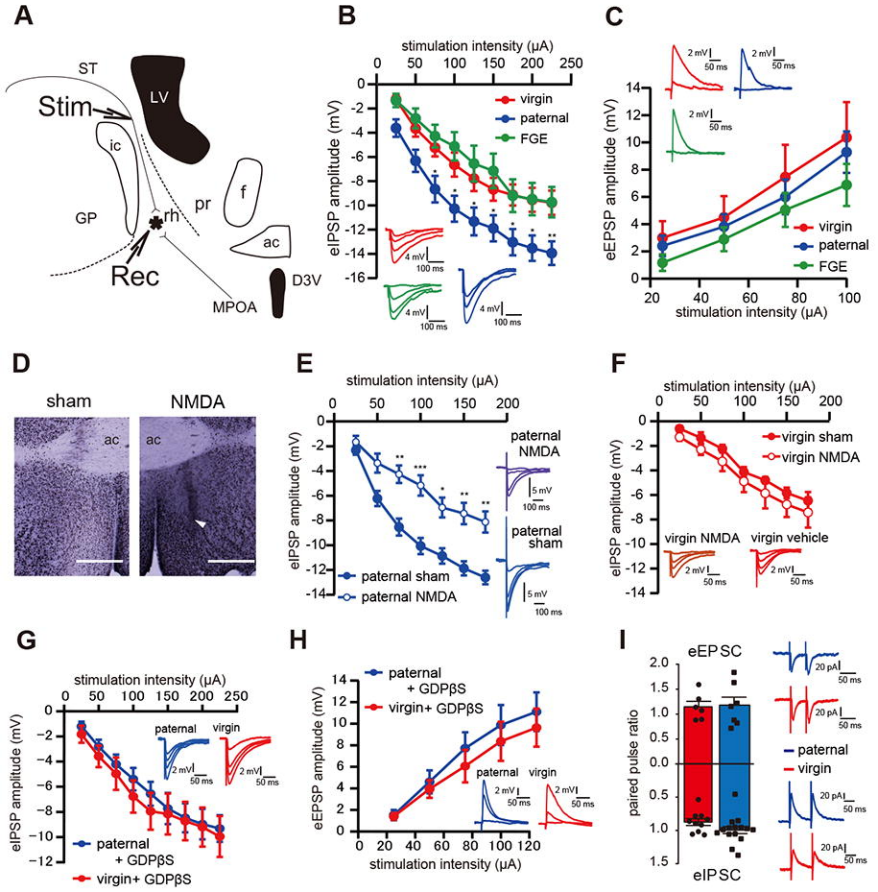
A
ST
Stim
LV
ic
GP
pr
rh
f
ac
Rec
MPOA
D3V
B
stimulation intensity (μA)
eIPSP amplitude (mV)
virgin
paternal
FGE
4 mV
100 ms
C
eEPSP amplitude (mV)
stimulation intensity (μA)
virgin
paternal
FGE
2 mV
50 ms
D
sham
NMDA
ac
E
stimulation intensity (μA)
eIPSP amplitude (mV)
paternal NMDA
paternal sham
5 mV
100 ms
F
stimulation intensity (μA)
eIPSP amplitude (mV)
virgin sham
virgin NMDA
virgin NMDA
virgin vehicle
2 mV
50 ms
G
stimulation intensity (μA)
eIPSP amplitude (mV)
paternal
virgin
paternal + GDPβS
virgin+ GDPβS
H
paternal + GDPβS
virgin+ GDPβS
eEPSP amplitude (mV)
stimulation intensity (μA)
paternal
virgin
2 mV
50 ms
I
eEPSC
eIPSC
paired pulse ratio
paternal
virgin
20 pA
50 ms
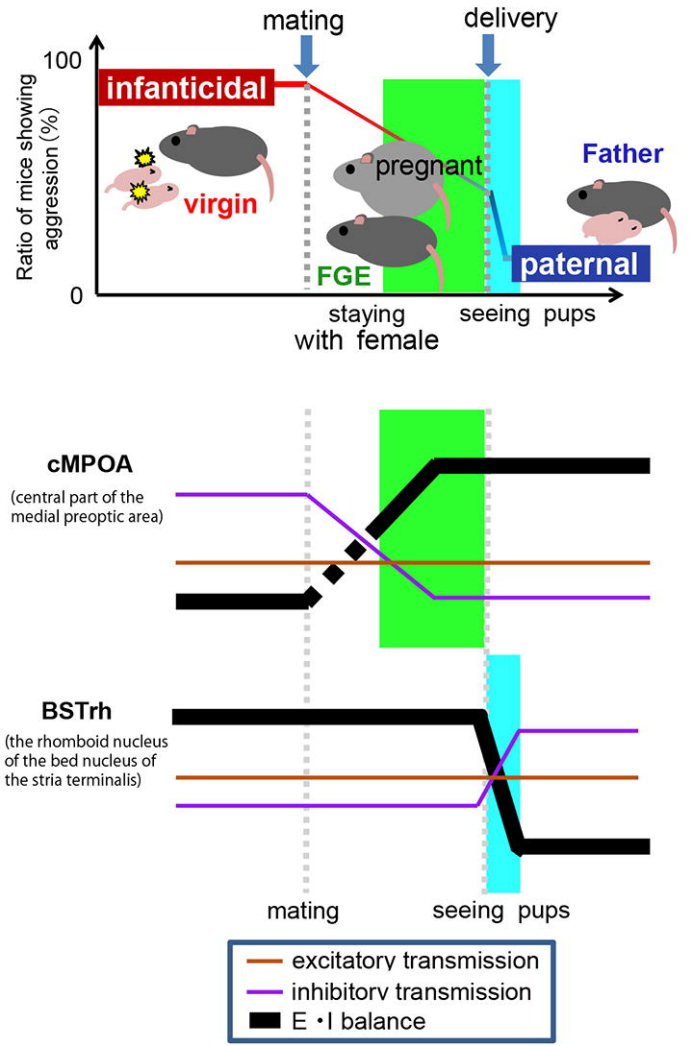
Graphical Abstract